Analog Network Coding Without Restrictions on Superimposed Frames

Xudong Wang, *Senior Member, IEEE*, and Wenguang Mao

***Abstract*—The applicability of analog network coding (ANC) to a wireless network is constrained by several limitations: 1) some ANC schemes demand fine-grained frame-level synchronization, which cannot be practically achieved in a wireless network; 2) others support only a specific type of modulation or require equal frame size in concurrent transmissions. In this paper, a new ANC scheme, called restriction-free analog network coding (RANC), is developed to eliminate the above limitations. It incorporates several function blocks, including frame boundary detection, joint channel estimation, waveform recovery, circular channel estimation, and frequency offset estimation, to support random concurrent transmissions with arbitrary frame sizes in a wireless network with various linear modulation schemes. To demonstrate the distinguished features of RANC, two network applications are studied. In the first application, RANC is applied to support a new relaying scheme called multi-way relaying, which significantly improves the spectrum efficiency as compared to two-way relaying. In the second application, RANC enables random-access-based ANC in an ad hoc network where flow compensation can be gracefully exploited to further improve the throughput performance. RANC and its network applications are implemented and evaluated on universal software radio peripheral (USRP) software radio platforms. Extensive experiments confirm that all function blocks of RANC work effectively without being constrained by the above limitations. The overall performance of RANC is shown to approach the ideal case of interference-free communications. The results of experiments in a real network setup demonstrate that RANC significantly outperforms existing ANC schemes and achieves constraint-free ANC in wireless networks.**

***Index Terms*—Analog network coding, channel estimation, frame-level synchronization, flow compensation, multi-way relaying.**

I. Introduction

ANALOG network coding (ANC) supports concurrent transmissions from two different transmitters to the same receiver. When one frame (called *self frame* in this paper) is known at the receiver, the other one (called *desired frame*) can be extracted from the superimposed signals by an ANC scheme. The assumption of knowing the self frame is valid in many scenarios of wireless networking, e.g., two-way relaying. Thus, it is highly beneficial to incorporate ANC into a wireless network to support concurrent transmissions and improve both spectrum efficiency and network capacity. However, little progress has been made so far to practically apply ANC to wireless networks. The difficulty is mainly attributed to the limitations in the existing ANC schemes.

To date, a number of ANC schemes have been developed. According to their limitations, these ANC schemes can be classified into two categories. The first category of ANC schemes demand a certain level of accuracy in frame-level synchronization between concurrent transmissions. In this category, some schemes such as amplify-and-forward two-way relaying [1] require strict synchronization. Such ANC is only applicable to a wireless network where all nodes in the network are strictly synchronized and network-wide packet scheduling is adopted. However, for many wireless networks such as ad hoc networks and mesh networks, it is impractical to implement network-wide packet scheduling or achieve strict synchronization among nodes. Other ANC schemes [2] of this category relaxed the requirement of synchronization by taking advantage of the cyclic prefix (CP) of orthogonal frequency-division multiplexing (OFDM) [3], [4]. As long as the misalignment of the two signals at the receiver does not exceed the length of the CP, there is no problem with frame reception. Unfortunately, if no global synchronization device like GPS is available, achieving synchronization accuracy of within one CP is highly challenging. Some researchers assume that short signaling messages (e.g., request to send (RTS)/clear to send (CTS) in IEEE 802.11) can be exchanged among nodes to achieve such a synchronization accuracy. However, this approach has been proved to be infeasible [5].

In the second category of ANC [6], concurrent transmissions can be totally asynchronous. However, a certain level of asynchronization is required to guarantee an interference-free part in a frame for two purposes: 1) identify the start (or the end) of a frame by matching a pilot sequence; 2) estimate channel distortion, frequency offset, and sampling offset. To ensure such an interference-free part, frame sizes in concurrent transmissions need to be equal; in case of unequal frame sizes, the shorter one must be padded to the same size of the longer one. Moreover, some random delay must be added by medium access control (MAC) before a transmission starts. Padding a shorter frame degrades spectrum efficiency, and inserting random delay does not really guarantee the required level of asynchronization in concurrent transmissions. Besides, this category of ANC is designed for a specific modulation scheme. For example, in [6], the design of ANC takes advantage of the features of minimum

Manuscript received November 08, 2013; revised June 11, 2014; October 14, 2014; and December 14, 2014; accepted December 17, 2014; approved by IEEE/ACM TRANSACTIONS ON NETWORKING Editor D. Goeckel. Date of publication January 27, 2015; date of current version April 14, 2016. This work was supported by the National Natural Science Foundation of China (NSFC) under Grant No. 61172066 and the Oriental Scholar Program of Shanghai Municipal Education Commission. *(Corresponding author: Xudong Wang,)*

The authors are with the University of Michigan–Shanghai Jiao Tong University Joint Institute, Shanghai Jiao Tong University, Shanghai 200240, China (e-mail: wxudong@ieee.org).

Color versions of one or more of the figures in this paper are available online at http://ieeexplore.ieee.org.

Digital Object Identifier 10.1109/TNET.2014.2385857

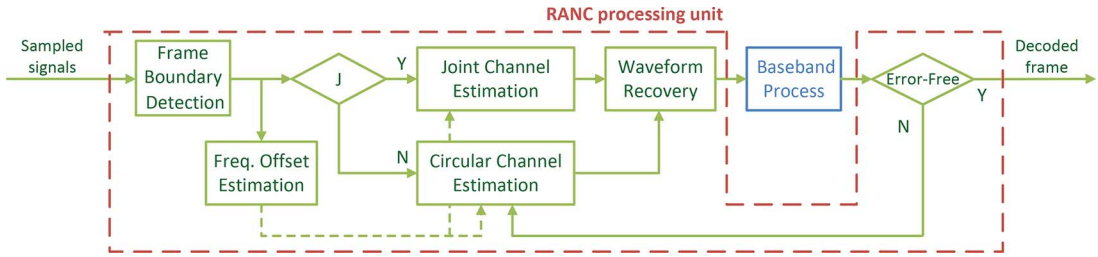

Fig. 1. Block diagram of a RANC receiver.

shift key (MSK) modulation, so it is inapplicable to other modulations schemes, including well-known ones like BPSK, QPSK, and QAM.

Due to the above constraints, the flexibility of incorporating ANC into a wireless network is highly limited. To utilize the benefits of ANC, such constraints need to be eliminated. In this paper, we propose a new ANC scheme to meet the following requirements: 1) Frame transmissions from two transmitters do not have any requirement of frame-level synchronization or asynchronization. 2) It is applicable to any linear modulation schemes such as BPSK, QPSK, and QAM. 3) It supports concurrent transmissions with unequal frame sizes. Therefore, the new scheme eliminates the constraints in existing ANC schemes so that two transmitting nodes can start cooperation without any restriction on superposition of two frames. With such a distinct advantage, it can be easily integrated with a random MAC protocol for scalable wireless networking. It can also be applied to many applications that demand restriction-free concurrent transmissions. As a result, this new ANC scheme is called a *restriction-free analog network coding* (RANC) scheme. RANC takes a receiver-oriented approach, i.e., major functions are located in the receiver. As shown in Fig. 1, the sampled superimposed signals are first forwarded to a frame boundary detection module to locate the starting and ending points of two frames superimposed as one. The frame boundary detection module also locates the samples that are helpful for channel estimation. To assist frame boundary detection at the receiver, a transmitter needs to form a frame following a certain format, as discussed in Section III-A. This is the only function that needs to be added to a RANC transmitter.

There are two channel estimation schemes in a RANC receiver: joint channel estimation and circular channel estimation. In the joint channel estimation module, channel coefficients for the self frame and the desired frame are estimated jointly by utilizing the samples located by the frame boundary detection module.

When the samples located by the frame boundary detection module are sufficient to obtain accurate channel coefficients with joint channel estimation, the interference to the desired frame can be canceled by completely removing the signals of the self frame. However, to compensate the shift of optimal sampling points, a waveform recovery module is needed to recover the waveform of the desired frame and then resample it. The samples from the waveform recovery module are finally used by a standard baseband module to reconstruct the desired frame.

When the samples located by the frame boundary detection module are insufficient, the decision block J selects the circular channel estimation module. Circular channel estimation takes multiple rounds of channel estimation to successively mitigate interference until the desired frame is error-free.

All algorithms adopted by the above function blocks are specially designed for realizing restriction-free ANC and hence do not need any level of synchronization (or asynchronization), require an interference-free part of a frame, or exploit the property of a specific modulation scheme. Thus, modulation-independent concurrent transmissions can be started *randomly* with *arbitrary* frame sizes.

With this new scheme, the applicability of analog network coding in wireless networks is significantly extended. In this paper, we study two applications of RANC. In the first application, RANC is applied to support a new relaying scheme called *multi-way relaying*. This scheme can achieve higher spectrum efficiency than that of two-way relaying when frames in a network have variable sizes. The second application of RANC is to enable effective random access in a wireless network with ANC. Due to the restriction-free characteristics of RANC, a novel mechanism called *flow compensation* becomes feasible in such networks. This mechanism significantly improves the network throughput when traffic flows in the network are not symmetric. Thus, in both applications, RANC brings many benefits that cannot be achieved by other ANC schemes. Moreover, with the constraint-free feature, RANC can be applied to many other applications in a creative way.

The entire scheme of RANC and its network applications are implemented and evaluated on a universal software radio peripheral (USRP)-based software radio testbed. First, each function block of RANC is validated. Results of experiments are compared to the case without such a function block. Comparisons illustrate that significant performance gain can be achieved by each function block. Experiments also confirm that the constraints in existing ANC schemes are completely eliminated in RANC. Second, the bit error rate (BER) performance of the entire RANC scheme is measured on the testbed. Results show that BER of decoding the desired frame from superimposed signals is close (within 0.3 dB) to the case of interference-free communications. Third, experiments for network applications of RANC are conducted in real networks deployed in our laboratory where flexibility and efficiency of applying RANC in wireless networks are clearly demonstrated. Evaluation results show that RANC improves throughput performance by 47%–80% in various scenarios.

The rest of the paper is organized as follows. The constraints of existing ANC schemes are investigated in Section II. System design, the major function blocks, and main features of RANC are presented in Section III. Network applications of RANC are proposed in Section IV. Implementation details are described

in Section V, and extensive experiments are conducted in Section VI. Related work is summarized in Section VII, and the paper is concluded in Section VIII.

II. Constraints in Analog Network Coding

The constraints that limit the applicability of ANC schemes are described in this section.

A. Synchronization

A simple ANC scheme is amplify-and-forward two-way relaying [1]. It requires perfect synchronization to achieve optimal performance. However, in a wireless network, it is difficult to achieve strict synchronization unless GPS or other global reference clock is available. Even if communication nodes are strictly synchronized, it is difficult to achieve frame-level synchronization, especially for data networks where transmissions are bursty. This issue is even more challenging for ad hoc networks where distributed scheduling is still a challenging issue.

To mitigate the issue of strict synchronization, an OFDM-based physical-layer network coding (PLNC) is proposed [2]. It requires the synchronization offset of two concurrent frames to be within the CP of an OFDM symbol. Such a scheme can be tailored for ANC. However, synchronization granularity within the length of a CP is still a challenging requirement in many communication systems. For example, the CP of an OFDM symbol in an 802.11a transceiver is specified as 0.8 μs [7]. As a result, two concurrent transmissions need to be synchronized within 0.8 μs, which is a nontrivial task. Without a GPS module, communication nodes have to rely on signaling messages to synchronize their transmissions. However, synchronization accuracy is limited by a few factors such as disparate processing time of an arrival message, propagation delay, and multipath effect. To the best of our knowledge, among all message-based synchronization schemes [5], [8], [9], the physical-layer reference broadcast scheme [5] achieves the highest accuracy, but the synchronization accuracy is only 1.85 μs (mean) $\pm$1.28 μs (deviation). Thus, satisfying the requirement of 0.8 μs synchronization accuracy is not practically feasible. As the physical layer keeps increasing the rate, the CP becomes even smaller. For example, the CP of an OFDM symbol in 802.11ad is 48.4 ns [10]. Achieving such a synchronization accuracy is so demanding even for GPS-based synchronization. A synchronization scheme called SourceSync [11] can achieve accurate symbol-level synchronization among multiple transmitting nodes to exploit sender diversity. In this scheme, a lead node starts its transmission first. Upon overhearing synchronization header from the lead node, other nodes join the transmissions sequentially so that all data frames can be seen as a single joint frame. When applying this scheme to ANC, there exist several limitations or issues. First, synchronization has to be triggered by the relay node since the two end nodes of ANC are usually hidden to each other. Second, since SourceSync has to be triggered by the relay node for ANC, it becomes inapplicable to either flow compensation or multi-way relaying, as explained in Section IV. Third, SourceSync needs a signaling protocol to constantly measure the propagation delay between different nodes, which results in overhead and is also complicated for hidden nodes. As a result, SourceSync does not really work in many scenarios of ANC.

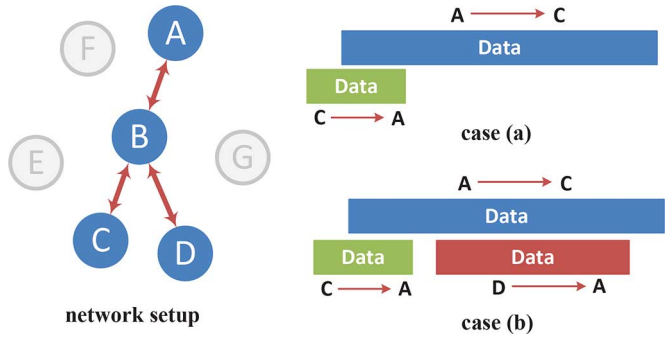

Fig. 2. Typical communication scenario in wireless networks.

B. Asynchronization and Frame Size

The ANC scheme in [6] requires an interference-free part (in the beginning or the end of a frame) for both frames. This part is for identifying the start (or the end) of a frame and also for estimating frequency offset, sampling offset, and channel distortion due to sudden frequency change. Thus, two frames to be transmitted have to maintain a certain level of asynchronization. To this end, the shorter frame has to be padded to the same length as the longer one. Moreover, a random delay must be inserted before a transmission starts. Padding frames leads to waste of transmission power and spectrum, and adding a random delay increases overhead. Moreover, inserting a random delay does not guarantee the two frames to be asynchronous with each other.

It should be noted that the interference-free part can be achieved at both frames even without frame padding. This occurs when two frames have a much different frame length. However, the spectrum utilization in this scenario is still low. Consider the example in Fig. 2, where Nodes A and C have frames to exchange with each other. We assume that the traffic from Node A to C and that from Node C to A belong to different applications, and hence frames sent from two nodes may have significantly different frame sizes [12]–[14]. We assume that the frame from Node C to A starts earlier to get an interference part but is shorter than the frame from Node A to C [see case (a)]. Thus, the frame from Node A to C can also get an interference part. When Node C finishes transmitting its frame, the channel from Node C to A becomes idle. However, even if the idle time is enough for Node D to send a frame to Node A, the transmission cannot proceed. The reason is as follows. If Node D starts its transmission during this idle time period, either Node A's or Node D's frame cannot have an interference-free part. As shown by case (b) in Fig. 2, when Node D's frame finishes earlier to allow an interference-free part in Node A's frame, then Node D's frame has no interference-free part. As a result, the idle time cannot be utilized even if it is enough for Node D to send a frame to Node A.

C. Modulation

Some ANC schemes are only applicable to a specific modulation scheme. The well-known ANC scheme in [6] relies on the

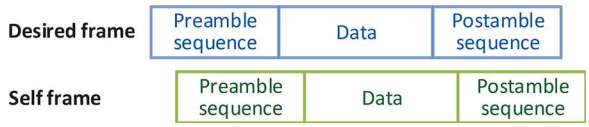

Fig. 3. Frame format of RANC.

property of the MSK modulation (i.e., signals have constant amplitude). With this property, when two MSK-modulated signals are superimposed asynchronously with each other, the amplitude for each signal can be easily estimated. Based on the amplitude knowledge of each signal, the superimposed signals can be decomposed based on the parallelogram law, and the possible phases for both signals can be determined [6]. Since the receiver gets the knowledge of one of signals, it can select the right phase of the other signal from the possible values. In the MSK modulation, information is carried by the phase difference between consecutive samples, and channel phase shift has no impact on the phase difference. Thus, the ANC scheme in [6] does not need a mechanism to track channel phase shift.

Considering many other modulation schemes (e.g., QAM), signal amplitude is not necessarily constant. Moreover, accurate phase tracking is needed for effective demodulation. Therefore, ANC schemes like [6] are not applicable to these modulations.

III. Restriction-Free Analog Network Coding

To eliminate constraints in existing ANC schemes, RANC is developed. Its major function blocks are described in this section.

A. Frame Boundary Detection

The frame boundary detection module detects the arrival of a superimposed frame, finds the starting and ending points of each frame in the superimposed signals, and locates useful samples for channel estimation. To this end, a frame format is designed as shown in Fig. 3 where two identical pseudo-random pilot sequences are attached to the header and the tail of a frame as the preamble and the postamble, respectively. Considering two transmitting nodes in a three-node setup of ANC, their pseudo-random pilot sequences need to be different. However, for the entire network, only two different pseudo-random pilot sequences are sufficient for the following reason. For a network, a MAC protocol is followed by communication nodes to form ANC cooperation groups, and each group does not interfere with any other groups. Thus, the pilot sequences of a group can be reused by another group.

A design of frame layout similar to Fig. 3 was first proposed in [15] and was also used in [6]. However, there exist a few differences between our scheme and the design in [6] and [15]. First, our design does not need extra header or trailer information at the end of a frame. Second, how to utilize the frame layout is significantly different. Specifically, the scheme in [6] requires an interference-free part at the preamble or the postamble of each frame in concurrent transmissions for timing synchronization and channel distortion evaluation. The scheme in [15] also expects a collision-free postamble when multiple transmissions collide. Instead, our scheme allows any degree of overlapping in two concurrently transmitted frames. With our frame layout, we can effectively utilize overlapping parts to estimate channel coefficients.

It should be noted that there exist some similarities between our design of preamble (or postamble) and DS-CDMA. we exploit the low cross-correlation property between preambles (or postambles) of concurrent transmitters to find the starting and ending points of each frame, while DS-CDMA relies on the same property to detect frames from different transmitters. However, there exist key differences. First, in RANC (and also other ANC schemes) only two transmitting users are considered in the same interference region, whereas DS-CDMA needs to support many users. Second, DS-CDMA is targeted toward the low data rate power-limited regime, whereas our scheme works in the bandwidth-limited high-data-rate regime. Due to such differences, we take a different approach (instead of DS-CDMA) to exploit the low cross-correlation property for RANC.

With the new frame format, two transmitters of a superimposed frame are required to adopt different pilot sequences. If the node (called *initiator*) that initiates RANC uses pilot sequence A, then the node (called *cooperator*) that cooperates with the initiator must use pilot sequence B. Since there exist only two transmitters in the same interference region, each node only needs to keep two different pilot sequences, one for its role of initiator and the other for its role of cooperator. As a result, two distinct pilot sequences are sufficient in the entire network, and they are known to any receiver. With distinct pilot sequences, the frames of concurrent transmissions can be detected via correlation. Let $\{p_{\rm s}[n]\}$ and $\{p_{\rm d}[n]\}$ denote two pilot sequences adopted by the self frame and the desired frame, respectively, and $\{s[n]\}$ stands for samples of the superimposed signals. To detect the two frames in the superimposed signals, the receiver correlates samples with two pilot sequences to get correlation sequences $\{S_{\rm s}[i]\}$ for the self frame and $\{S_{\rm d}[i]\}$ for the desired frame, i.e.,

$$S_{\rm s}[i] = \sum_{k=0}^{L-1} s[i+k]p_{\rm s}[k+1]$$
$$S_{\rm d}[i] = \sum_{k=0}^{L-1} s[i+k]p_{\rm d}[k+1].$$

The value of correlation spikes only when the sequence $\{p_{\rm s}[n]\}$ or $\{p_{\rm d}[n]\}$ perfectly aligns with the preamble or the postamble of the corresponding frame. Hence, frame boundary detection can be fulfilled by checking the peaks of correlation: 1) the first peak indicates the arrival of a superimposed frame; 2) the peaks of $\{S_{\rm s}[i]\}$ locate the beginning and the end of the self frame; 3) the peaks of $\{S_{\rm d}[i]\}$ tell the beginning and the end of the desired frame. Note that although the preamble (or the postamble) of one frame may be interfered by the other frame, the impact of the interference on the occurrence of correlation peaks is negligible. This observation has been verified by experiments in [16] and [17].

Based on the located points in each frame, we need to identify samples that can be utilized to estimate channel coefficients. For

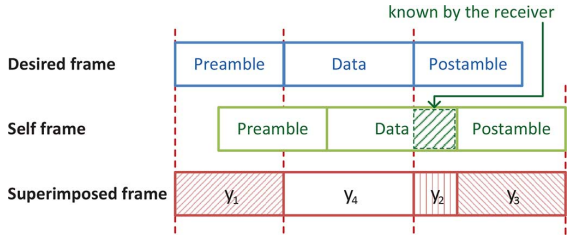

Fig. 4. Different samples detected by the frame boundary detection module.

joint channel estimation, the samples that can be used must satisfy the following condition: In each sample, the corresponding symbols from both frames are known by the receiver. We call these samples *useful samples*. To this end, the superimposed frame is split into several parts as shown in Fig. 4: 1) $\mathbf{y_1}$ is aligned with the preamble of the desired frame; 2) $\mathbf{y_2}$ is in between the two starting points of the postamble of the two frames; 3) $\mathbf{y_3}$ is the samples aligned with the postamble of the self frame; 4) $\mathbf{y_4}$ takes the remaining part. Whether these parts of the superimposed frame can be utilized for joint channel estimation is analyzed below.

Considering samples $\mathbf{y_1}$ with a length of N_1, we have[1]

$$y_1[n] = h_{\mathrm{d,eqv}} x_{1d}[n] + h_{\mathrm{s,eqv}} x_{1s}[n] + w_1[n], \quad n = 1, \ldots, N_1$$

where $h_{\mathrm{s,eqv}}$ and $h_{\mathrm{d,eqv}}$ are the equivalent channel coefficients in the discrete-time baseband model for the self frame and the desired frame, $x_{1d}[n]$ and $x_{1s}[n]$ are symbols in two frames, and $w_1[n]$ is noise. Note that $\{x_{1d}[n]\}$ is the preamble of the desired frame, so it is known. Moreover, $\{x_{1s}[n]\}$ is a sequence with a number of zeros followed by the truncated preamble sequence of the self frame. Since the receiver has located the starting point of each frame, the shift (in samples) between two frames, namely the number of zeros (denoted by N_{1z}) in $\{x_{1s}[n]\}$ before the truncated preamble sequence, is known. Thus, the receiver has the full knowledge of the sequence $\{x_{1s}[n]\}$. As a result, $\mathbf{y_1}$ is useful for estimating channel coefficients $h_{\mathrm{s,eqv}}$ and $h_{\mathrm{d,eqv}}$. A similar analysis on $\mathbf{y_3}$ indicates that $\mathbf{y_3}$ can also be used for channel estimation. Furthermore, samples in $\mathbf{y_2}$ can be expressed as

$$y_2[n] = h_{\mathrm{d,eqv}} x_{2d}[n] + h_{\mathrm{s,eqv}} x_{2s}[n] + w_2[n], \quad n = 1, \ldots, N_2$$

where N_2 is the length of the samples $\mathbf{y_2}$. Note that $\{x_{2d}[n]\}$ is the first N_2 symbols of the postamble of the desired frame, and hence is fully known by the receiver. $\{x_{2s}[n]\}$ is a part of payload of the self frame, so it is known by the receiver. Therefore, $\mathbf{y_2}$ is also useful for channel estimation. However, samples y_4 involve unknown symbols in the data field of the desired frame, so they cannot be used for joint channel estimation. It should be noted that whether the self frame or the desire frame starts earlier does not matter; the above analysis is still applicable.

As shown in Fig. 4, only partial preamble of the self frame is located in $\mathbf{y_1}$, but the entire preamble of the desired frame lies in this region. Thus, if $\mathbf{y_1}$ is used for channel estimation, a higher accuracy can be achieved for the channel coefficients of the desired frame since the first N_{1z} samples in $\mathbf{y_1}$ make no contribution to the accuracy of estimating channel coefficients of the self frame. To quantify the quality of samples for channel estimation, we define *effective samples* as follows: Considering a useful sample for channel estimation, if its component of the self frame (or the desired frame) is nonzero, then it is an *effective sample* for the self frame (or the desired frame). Given all useful samples, the number of effective samples for the desired frame is always equal to the total size of pilot sequences (denoted by N_{p}) since all samples aligning with the preamble and the postamble of the desired frame are *useful* and *effective* for estimating its channel coefficients. However, the number of effective samples for the self frame can be small. Thus, the number of effective samples in the self frame is a critical parameter for channel estimation. If it is greater than a threshold N_{t} (i.e., Condition J in Fig. 1), then the useful samples are sufficient for jointly estimating channel coefficients of both the desired frame and the self frame. In this case, a joint channel estimation module is employed. However, the effective samples for the self frame can be very small in some cases. For example, the self frame is short and lies within the data range of the desired frame. To solve this problem, another channel estimation scheme, called circular channel estimation, is needed. Its details are presented in Section III-D. The threshold N_{t} for selecting joint channel estimation or circular channel estimation is a system parameter. It can be determined based on testing results of RANC, as discussed in Section VI.

B. Joint Channel Estimation

As discussed before, if both the self frame and the desired frame have enough effective samples, the joint channel estimation scheme is adopted.

Considering a superimposed frame, if channel estimation is conducted separately for each frame by taking the other frame as interference, then the estimation accuracy is low because the interference is too strong. One solution to this problem is to impose an interference-free part at the preamble (or the postamble) of each frame to guarantee that the channel estimation can be conducted without interference. However, this solution leads to restrictions on the applicability of ANC as discussed in Section II-B. In our scheme, instead of requiring interference-free samples, we utilize the overlapping part of two frames to jointly estimate the channel coefficients by exploiting the frame layout and the knowledge of the self frame.

Assuming that both the self frame and the desired frame adopt linear modulations, the waveform of the superimposed frame at the receiver can be expressed as

$$y(t) = \sum_{\substack{n > \frac{t}{T} - n_h + 1, \\ n \leqslant \frac{t}{T} + 1}} h_{\mathrm{d}} x_{\mathrm{d}}[n] g_{\mathrm{d}}(t - (n-1)T) + \sum_{\substack{n > \frac{t - T_{\mathrm{d}}}{T} - n_h + 1, \\ n \leqslant \frac{t - T_{\mathrm{d}}}{T} + 1}} h_{\mathrm{s}} x_{\mathrm{s}}[n] g_{\mathrm{s}}(t - (n-1)T - T_{\mathrm{d}}) + w(t)$$

where T is the symbol time, n is an integer number, h_{d} and h_{s} denote the channel gains of the desired frame and the self

[1]For the sake of clarity, the items caused by multipath effect are omitted in the following equations.

frame, respectively, $\{x_{\rm d}[n]\}$ and $\{x_{\rm s}[n]\}$ stand for the symbol sequences of the two frames, $g_{\rm d}(t)$ and $g_{\rm s}(t)$ represent pulse shapes of the two frames, and $T_{\rm d}$ denote the time offset between the two frames. $w(t)$ is the noise process. Also, n_h, which is the number of channel taps, captures the intersymbol interference (ISI) and the multipath effect. Upon sampling, the signal of the ith sample is given by

$$\begin{aligned} y[i] = &\sum_{\substack{n>\frac{\Delta}{T}-n_h+i,\\ n\leqslant\frac{\Delta}{T}+i}} h_{\rm d}x_{\rm d}[n]g_{\rm d}((i-1)T+\Delta-(n-1)T) \\ &+\sum_{\substack{n>i-n_h-\frac{T_{\rm d}-\Delta}{T},\\ n\leqslant i-\frac{T_{\rm d}-\Delta}{T}}} h_{\rm s}x_{\rm s}[n]g_{\rm s}((i-1)T+\Delta-(n-1)T \\ &-T_{\rm d})+w((i-1)T+\Delta) \end{aligned}$$

where $(i-1)T+\Delta$ is the sampling position. In a conventional point-to-point communication mode, Δ is locked to a value that corresponds to the optimal sampling position via a timing synchronization mechanism [18]. However, in a superimposed frame, timing synchronization signals of one frame is interfered by the other frame. Tracking the optimal sampling positions is infeasible since Δ may vary from one round of transmissions to another. It is also difficult to precisely determine Δ.

For convenience, let $D=\lceil (T_{\rm d}-\Delta)/T\rceil$ and $\delta = DT-(T_{\rm d}-\Delta)$. Thus, a sample can be described as

$$\begin{aligned} y[i] = &\sum_{n=0}^{n_h-1} h_{\rm d}x_{\rm d}[i-n]g_{\rm d}(\Delta+nT) \\ &+\sum_{n=0}^{n_h-1} h_{\rm s}x_{\rm s}[i-n-D]g_{\rm s}(\delta+nT) \\ &+w(iT-T+\Delta). \end{aligned} \tag{1}$$

In matrix form, it is

$$\mathbf{y}=[\mathbf{X_d}\mathbf{X_s}]\begin{bmatrix}\mathbf{h_{d,eqv}}\\ \mathbf{h_{s,eqv}}\end{bmatrix}+\mathbf{w}, \tag{2}$$

where $\mathbf{y}$ contains N samples of the entire superimposed frame, $\mathbf{X_d}$ and $\mathbf{X_s}$ are $N\times n_h$ matrices whose columns are shifted versions of $\{x_{\rm d}[n]\}$ and $\{x_{\rm s}[n]\}$, respectively, and $\mathbf{w}$ is an N-dimension column vector that represents the noise. Moreover, the n_h-dimension vectors $\mathbf{h_{d,eqv}}$ and $\mathbf{h_{s,eqv}}$ are the equivalent channel coefficients for the desired frame and the self frame in the discrete-time baseband model. It can be shown that

$$\begin{cases}\mathbf{h_{d,eqv}}=h_{\rm d}\left[g_{\rm d}(\Delta)g_{\rm d}(\Delta+T)\ldots g_{\rm d}(\Delta+(n_h-1)T)\right]^{\mathsf{T}}\\ \mathbf{h_{s,eqv}}=h_{\rm s}\left[g_{\rm s}(\delta)g_{\rm s}(\delta+T)\ldots g_{\rm s}(\delta+(n_h-1)T)\right]^{\mathsf{T}}.\end{cases}$$

The above equation indicates that the equivalent channel coefficients depend on both channel fading and pulse shape values at the sampling points. Hence, the equivalent channel coefficients vary from time to time, even if the channels are stationary. Thus, online channel estimation is indispensable.

Since samples $\mathbf{y_1}$, $\mathbf{y_2}$, and $\mathbf{y_3}$ in Fig. 4 are part of the N-dimension vector $\mathbf{y}$, a formula similar to (2) can be written as

$$\begin{bmatrix}\mathbf{y_1}\\ \mathbf{y_2}\\ \mathbf{y_3}\end{bmatrix}=\mathbf{C_{est}}\begin{bmatrix}\mathbf{h_{d,eqv}}\\ \mathbf{h_{s,eqv}}\end{bmatrix}+\begin{bmatrix}\mathbf{w_1}\\ \mathbf{w_2}\\ \mathbf{w_3}\end{bmatrix} \tag{3}$$

where the matrix $\mathbf{C_{est}}$ consists of submatrices of $[\mathbf{X_d}\mathbf{X_s}]$ that correspond to $\mathbf{y_1}$, $\mathbf{y_2}$, and $\mathbf{y_3}$. As discussed in Section III-A, symbols of the desired frame and the self frame that are aligned with $\mathbf{y_1}$, $\mathbf{y_2}$, and $\mathbf{y_3}$ are known by the receiver, so the receiver has the full knowledge of the matrix $\mathbf{C_{est}}$. Therefore, (3) can be utilized to jointly estimate channel coefficients of the desired frame and the self frame. Based on least square estimation, the equivalent channel coefficients are estimated as

$$\begin{bmatrix}\tilde{\mathbf{h}}_{\mathbf{d,eqv}}\\ \tilde{\mathbf{h}}_{\mathbf{s,eqv}}\end{bmatrix}=(\mathbf{C_{est}}^H\mathbf{C_{est}})^{-1}\mathbf{C_{est}}^H\begin{bmatrix}\mathbf{y_1}\\ \mathbf{y_2}\\ \mathbf{y_3}\end{bmatrix}.$$

Note that the inverse matrix of $\mathbf{C_{est}}^H\mathbf{C_{est}}$ exists if and only if the matrix $\mathbf{C_{est}}$ has a full rank. This can be guaranteed by selecting different pilot sequences for the two frames such that any column in the matrix $\mathbf{C_{est}}$ cannot be expressed as a linear combination of other columns.

C. Waveform Recovery and Resampling

Given the channel coefficients, the RANC receiver removes the signals of the self frame from the superimposed frame as follows:

$$\begin{aligned}\mathbf{y_d}&=\mathbf{y}-\mathbf{X_s}\tilde{\mathbf{h}}_{\mathbf{s,eqv}}\\ &=\mathbf{X_d}\mathbf{h_{d,eqv}}+\mathbf{X_s}(\mathbf{h_{s,eqv}}-\tilde{\mathbf{h}}_{\mathbf{s,eqv}})+\mathbf{w}\\ &=\mathbf{X_d}\mathbf{h_{d,eqv}}+\tilde{\mathbf{w}},\end{aligned} \tag{4}$$

where $\tilde{\mathbf{w}}$ is the residual interference plus noise. The interference-canceled signal $\mathbf{y_d}$ cannot be directly used for demodulation because the sampling points in $\mathbf{y_d}$ may be shifted from the optimal positions of the desired frame. Thus, we first recover the waveform of the desired frame from $y_{\rm d}$ as

$$\begin{aligned}\tilde{y}_{\rm d}(t)&=\sum_{n=1}^{N}y_{\rm d}[n]{\rm sinc}\left(\frac{t-nT}{T}\right)\\ &\approx\sum_{n:|t-nT|\leqslant 6T}y_{\rm d}[n]{\rm sinc}\left(\frac{t-nT}{T}\right)\end{aligned}$$

where the approximation is proper, since sinc signals outside an internal of $6T$ are negligible. To minimize the distortion of the recovered waveform, an oversampling mechanism is adopted, i.e., superimposed signals are oversampled before they are forwarded to frame boundary detection module as shown in Fig. 1. If a root-raised-cosine pulse shape is adopted by the two transmitters, an oversampling rate of twice of the symbol rate is sufficient. In this case, symbol time T in the above equation needs to be replaced by $T/2$.

After the waveform recovery, the resampling process is conducted. In this process, a timing synchronization algorithm [18] is applied to relocate the optimal sampling points of the desired frame.

D. Circular Channel Estimation

When the size of the self frame is less than that of the desired frame, the number of effective samples for the self frame (marked by l_1 and l_2) can be small as shown in Fig. 5. If the size of the self frame further drops, it is possible that l_1 and l_2 in Fig. 5 approach zero. In this case, the channel coefficients cannot be accurately estimated through joint channel estimation.

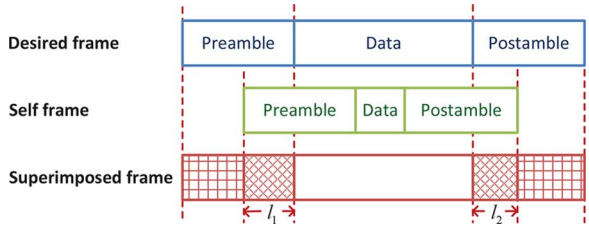

Fig. 5. Insufficient effective samples for the self frame.

Considering arbitrary frame sizes in concurrent transmissions, such an event can easily occur.

To address the above issue, circular channel estimation is required. It is based on the concept of successive interference mitigation. In the first step, a preliminary channel estimation is performed for channel coefficients of the self frame. Since joint channel estimation is not effective for the self frame when its number of effective samples is low, a conventional approach is adopted, i.e., estimating the channel coefficients of the self frame by considering the desired frame as interference. In the second step, the joint channel estimation algorithm is applied to estimate the channel coefficients of the desired frame. We know that the number of effective samples for the desired frame is always sufficient (i.e., equal to the number of symbols in the pilot sequences). Thus, the joint channel estimation algorithm is always effective for estimating channel coefficients of the desired frame. In the third step, the receiver performs waveform recovery and resampling as described in Section III-C. Since the channel coefficients of the self frame are not accurate, according to (4), the interference from the self frame cannot be fully removed. The remaining interference degrades the signal-to-interference-plus-noise ratio (SINR) of the desired frame and probably leads to decoding errors. However, the erroneous decoded data are useful. In fact, after decoding, the receiver obtains a symbol sequence, which is an approximation to the desired frame.[2] Instead of providing the decoded results to the upper layer, the receiver feeds the approximate symbol sequence back to the circular channel estimation module, as shown in Fig. 1. In this new round of channel estimation, the interference in estimating the channel coefficients of the self frame in samples $\mathbf{y}$ can be mitigated. The new samples $\mathbf{y_{s,est}}$ are equal to $\mathbf{y} - \tilde{\mathbf{X}}_\mathbf{d}\tilde{h}_{\mathrm{d,eqv}}$, where $\tilde{\mathbf{X}}_\mathbf{d}$ are symbols (i.e., approximate ones of the desired frame) organized in a matrix format as defined in the channel model in (2). Since the receiver has accurately estimated the channel coefficients for the desired frame, we have

$$\begin{aligned}\mathbf{y_{s,est}} &= \mathbf{X_s h_{s,eqv}} + \mathbf{X_d}(\mathbf{h_{d,eqv}} - \tilde{\mathbf{h}}_\mathbf{d,eqv}) \\ &\quad + \tilde{\mathbf{h}}_\mathbf{d,eqv}(\mathbf{X_d} - \tilde{\mathbf{X}}_\mathbf{d}) + \mathbf{w} \\ &\approx \mathbf{X_s h_{d,eqv}} + \tilde{\mathbf{h}}_\mathbf{d,eqv}(\mathbf{X_d} - \tilde{\mathbf{X}}_\mathbf{d}) + \mathbf{w} \\ &= \mathbf{X_s h_{s,eqv}} + \tilde{\mathbf{h}}_\mathbf{d,eqv}\mathbf{X_e} + \mathbf{w}\end{aligned}$$

where the error sequence $\mathbf{X_e}$ is defined as $\mathbf{X_d} - \tilde{\mathbf{X}}_\mathbf{d}$. Although symbols from the decoded results are not perfect, they help dramatically mitigate the interference in estimating the channel coefficients for the self frame. An illustrative example showing the original interference and the residual interference after mitigation is given in Fig. 6. Thus, based on samples $\mathbf{y_{s,est}}$, the performance of estimating channel coefficients of the self frame is highly improved. The procedure discussed previously may repeat several rounds, and the estimation accuracy of the channel coefficients of the self frame will be increased round by round, which eventually leads to accurate samples of the desired frame (i.e., $\mathbf{y_d}$). Based on these samples, the waveform recovery module achieves successful reception of the desired frame. According to the results of experiments in Section VI-A.4, two rounds of circular channel estimation are sufficient to achieve successful decoding for low-order modulation schemes such as BPSK and QPSK. For higher-order modulations, more rounds are needed.

[2]Due to the page limit, the proof is omitted, and the detailed derivation and explanation can be found in [19, Appendix]

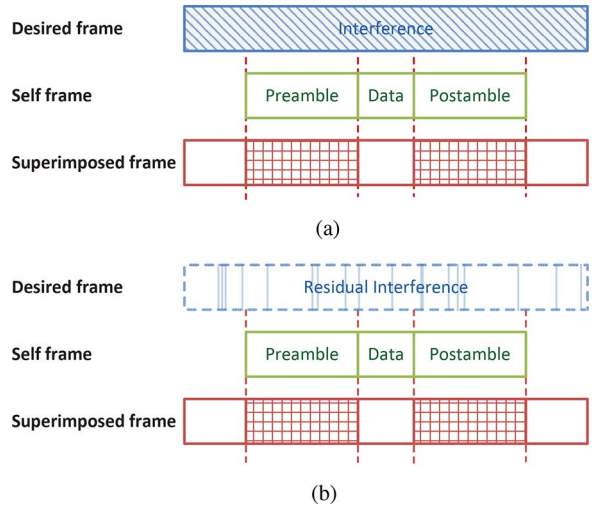

Fig. 6. Circular channel estimation. (a) First channel estimation for the self frame (the desired frame is interference). (b) Second channel estimation for the self frame (interference from the desired frame is mitigated).

E. Frequency Offset

In the previous sections about channel estimation, the carrier frequency at the receiver is assumed to be the same as that in the transmitters. However, transceivers in commercial communications usually do not have such high performance in carrier frequency stability. As a result, there exists a frequency offset between the actual received signal and the original signal. Suppose f_s is the frequency offset between the receiver and the transmitter of the self frame and f_d is the frequency offset for the desired frame. Thus, given a sample $y[i]$ with symbol period T, we have

$$\begin{aligned}y[i] = &\sum_{k=0}^{n_h-1} h_{\mathrm{d,eqv}}[k+1]x_\mathrm{d}[i-k]e^{j2\pi f_\mathrm{d} iT} \\ &+ \sum_{k=0}^{n_h-1} h_{\mathrm{s,eqv}}[k+1]x_\mathrm{s}[i-k-D]e^{j2\pi f_\mathrm{s} iT} + w[n].\end{aligned}$$

Thus, the frequency offset changes the equivalent channel coefficients in (1). If it is not compensated, the performance of interference cancellation drops. Moreover, the frequency offset between two devices varies from time to time. Thus, it needs to

be estimated and compensated for each reception of superimposed frames. There exist frequency offset estimation schemes for superimposed frames [6], [16], [20], but they do not work for RANC. The reason is that schemes in [6] and [16] rely on the existence of an interference-free part in a superimposed frame, and the scheme in [20] assumes frame-level synchronization. Thus, a new frequency offset estimation scheme is developed as follows.

Since the frequency offset estimation for both $f_{\rm s}$ and $f_{\rm d}$ follows the same approach, we take $f_{\rm s}$ as an example to describe our frequency offset estimation scheme.

Considering the preamble sequence $\{p_{\rm s}[i]\}$ of the self frame, its length is L_p (i.e., $N_p/2$), and it starts from index i_1 in the sample sequence $\{y[i]\}$, which is determined in the frame boundary detection module. Suppose the frequency offset used for compensating the self frame is $\tilde{f}_{\rm s}$, then the correlation between the preamble and the samples that align with the preamble is

$$\begin{aligned} V_1 &= \sum_{i=i_1}^{i_1+L_p-1} y[i] \times p_{\rm s}[i-i_1+1] e^{-j2\pi \tilde{f}_{\rm s} iT} \\ &\approx \sum_{i=i_1}^{i_1+L_p-1} h_{\rm s,eqv}[1] x_{\rm s}[i-D] e^{j2\pi(f_{\rm s}-\tilde{f}_{\rm s})iT} p_{\rm s}[i-i_1+1] \\ &= \sum_{i=i_1}^{i_1+L_p-1} h_{\rm s,eqv}[1] (p_{\rm s}[i-i_1+1])^2 e^{j2\pi(f_{\rm s}-\tilde{f}_{\rm s})iT} \\ &= h_{\rm s,eqv}[1] e^{j2\pi(f_{\rm s}-\tilde{f}_{\rm s})i_1 T} \sum_{i=0}^{L_p-1} e^{j2\pi(f_{\rm s}-\tilde{f}_{\rm s})iT}. \end{aligned}$$

Only the first item of $\mathbf{h_{s,eqv}}$, i.e., $h_{\rm s,eqv}[1]$, is considered in the above equations because multipath and ISI items are eliminated by correlation with the pseudo-random sequence. Moreover, the approximation in the above equations is valid because the contribution from $x_{\rm d}[n]$ and $w[n]$ can be neglected due to the pseudo-noise nature of preamble. Suppose the estimated frequency offset $\tilde{f}_{\rm s}$ is very close to the actual value $f_{\rm s}$, then $(f_{\rm s}-\tilde{f}_{\rm s})\cdot iT \approx 0$ when i is small, e.g., for $i \leqslant L_p-1$. However, i_1 can be a number much larger than L_p, so $(f_{\rm s}-\tilde{f}_{\rm s})\cdot i_1 T$ does not really approach zero. Hence, the correlation V_1 becomes

$$V_1 \approx L_p h_{\rm s,eqv}[1] e^{j2\pi(f_{\rm s}-\tilde{f}_{\rm s})i_1 T}.$$

Similarly, the correlation between the postamble of the self frame and samples that align with the postamble has the following result:

$$V_2 \approx L_p h_{\rm s,eqv}[1] e^{j2\pi(f_{\rm s}-\tilde{f}_{\rm s})i_2 T}$$

where i_2 is the sample index at which the postamble of the self frame starts. Based on the above equations, V_1 and V_2 are actually two vectors with approximately equal amplitude, and their phase offset is $\alpha = 2\pi(f_{\rm s}-\tilde{f}_{\rm s})(i_2-i_1)T$, as shown in Fig. 7. When the phase offset is equal to zero, the amplitude of V_1+V_2 reaches the maximum. Since i_2-i_1 is the number of symbols in the payload and is nonzero, the maximal amplitude of V_1+V_2 is achieved when $\tilde{f}_{\rm s} = f_{\rm s}$. This condition means

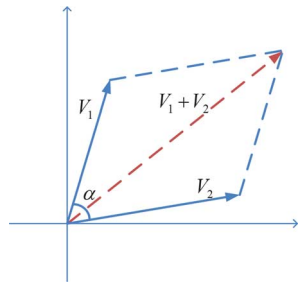

Fig. 7. Relationship between correlations V_1 and V_2.

that we can vary the values of $\tilde{f}_{\rm s}$ to search the real frequency offset $f_{\rm s}$ by checking if V_1+V_2 reaches the maximum. However, when $|f_{\rm s}-\tilde{f}_{\rm s}|$ equals a multiple of $\Delta f = \frac{1}{(i_2-i_1)T}$, V_1+V_2 also reaches the maximum. These cases cause confusion to the above approach of frequency offset searching. Fortunately, this confusion can be eliminated by narrowing the searching range of frequency offset. Suppose we start from a preliminary frequency offset $f_{\rm s,est}$, which is usually obtained through a preliminary frequency offset estimation scheme. If $|f_{\rm s}-f_{\rm s,est}| \leqslant \frac{\Delta f}{2}$ and the searching range is $[f_{\rm s,est}-\frac{\Delta f}{2}, f_{\rm s,est}+\frac{\Delta f}{2}]$, then we know that $\tilde{f}_{\rm s}-f_{\rm s}$ varies within $(-\Delta f, \Delta f)$. Thus, V_1+V_2 can only reach the maximum when $\tilde{f}_{\rm s} = f_{\rm s}$. In other words, the frequency offset can be accurately determined without any confusion. The condition of $|f_{\rm s}-f_{\rm s,est}| \leqslant \frac{\Delta f}{2}$ can be easily maintained in a practical system. We will validate this assumption in Section VI through experiments.

The above analysis leads to the following frequency offset estimation scheme. Initially, a preliminary frequency offset estimation $f_{\rm s,est}$ is conducted with an interference-free frame during the signaling process. Upon RANC starts, the frequency offset estimated in the previous transmission is used as the preliminary frequency offset for the next transmission. In case no transmission occurs for a time period longer than a few seconds, then the signaling process is followed to conduct frequency offset estimation with an interference-free frame. Thus, $|f_{\rm s}-f_{\rm s,est}| \leqslant \frac{\Delta f}{2}$ is always satisfied. Second, starting from $f_{\rm s,est}$, $\tilde{f}_{\rm s}$ varies by a step size of δ_f within $(-\frac{\Delta f}{2}, \frac{\Delta f}{2})$. When V_1+V_2 reaches the maximum, $\tilde{f}_{\rm s}$ gives an accurate estimation of the real frequency offset for the self frame. The step size δ_f is much smaller than Δf, and it can be fine-tuned as a system parameter.

IV. Network Applications of RANC

Without requiring frame-level synchronization, an interference-free part for each frame in concurrent transmission, or a specific modulation scheme, RANC significantly extends the applicability of ANC to wireless networks. In this section, two applications of RANC are provided. The first one is using RANC to support a new relaying strategy called *multi-way relaying*. Compared to two-way relaying, this strategy further improves the spectrum utilization when there are variable frame sizes in networks. The second application of RANC is to enable random access in a wireless network with ANC. Both applications become feasible thanks to the constraint-free feature of RANC.

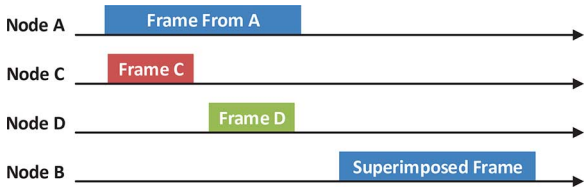

Fig. 8. Flow diagram of multi-way relaying.

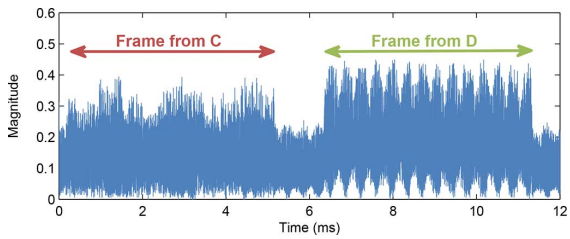

Fig. 9. Snapshot of the superimposed signals at Node B during the transmission period of a frame from Node A. These signals are sampled in a USRP device.

A. Multi-Way Relaying in Wireless Networks

The example discussed in Section II-B indicates that current ANC schemes, which require synchronization or sufficient interference-free parts, only support two frames concurrently transmitted to the relay node (known as *two-way relaying*). This pattern of cooperation is not efficient when the sizes of two frames are significantly different as mentioned in the example.

To further improve the spectrum utilization of a relay network, we propose a new cooperation strategy called *multi-way relaying*, which is supported by RANC. With this strategy, Node D starts its transmission once the frame from Node C is completely transmitted as shown in Figs. 8 and 9. After the transmission of Node D is finished, the relay node (e.g., Node B) amplifies and forwards the superimposed signals to Nodes A and C. Since no synchronization or interference-free parts are required, RANC can be used to decode the desired frames for Node A and Node C, respectively. Taking Node C as an example, the details of the decoding procedure are discussed as follows.

- To cancel all the interference when receiving the frame from Node A, Node C has to overhear the frame transmitted by Node D. Usually, if Node D is close to Node C, the signal from Node A, which is two hops away from Node C, will be dominated by that from Node D. In this case, the probability of successful overhearing is high.
- To support frame boundary detection, frames from Node C and Node D can share the same pilot sequence, but the frame from Node A needs to adopt a different one.
- The channel coefficients for the frame from Node A are estimated by utilizing the joint channel estimation scheme, while those for the frames from Nodes C and D are determined by the circular channel estimation scheme.

Although there are two frames (from Nodes C and D) sequentially superimposed with the frame from Node A in our example, frames from more nodes can be involved if the length of the frame from Node A is longer, and the decoding procedure described above is still applicable. Since the frames concurrently transmitted to the relay node come from multiple nodes, we call the scheme *multi-way relaying*. In this network application, the second and the following short frames (to Node A) are started while the long frame (from Node A to C) is in the middle of transmission, so synchronization schemes like SourceSync [11] are not applicable.

B. Random Access With RANC

Enhancing the throughput of a wireless network with random access is an important problem. One effective solution to this problem is to incorporate advanced physical-layer transmission technique into such networks. Since ANC can significantly improve the spectrum utilization and hence the network throughput, applying ANC to random access of wireless networks is beneficial. However, the existing ANC schemes are difficult to be applied to a random access protocol. In contrast, RANC can be easily applied to such a scenario for the following reasons. First, most ANC schemes, such as that in [2], require a certain level of synchronization among different nodes. However, the accuracy of existing synchronization schemes for random access networks, including the reference broadcast technique [5] that exploits signaling messages (such as RTS, CTS) to synchronize two nodes, can hardly reach the requirement imposed by these ANC schemes. RANC supports fully asynchronous transmissions, and hence the synchronization requirement is completely eliminated. Second, some ANC schemes, such as that in [6], require a specific modulation, while RANC supports all linear modulation schemes, including those adopted by IEEE 802.11 (i.e., BPSK, QPSK, 16QAM, and 64QAM). This feature allows RANC to be easily applied to many scenarios such as IEEE 802.11 networks and cellular networks. Third, due to the constraint-free feature, RANC provides more freedom in designing random access mechanisms for improving the network performance. To demonstrate flexibility and efficiency of integrating RANC with random access networks, a simple MAC protocol integrating RANC is proposed below. It matches the mechanisms of IEEE 802.11 DCF. We first present the protocol without considering hidden terminals. How to resolve the hidden terminal issue is discussed in the end of this section.

1) Forming ANC Cooperation: The key issue in designing a random access protocol with RANC is how to dynamically form ANC cooperation groups among network nodes according to traffic demands. In our MAC protocol, we exploit signaling frames such as RTS and CTS to form ANC cooperation groups. Consider that a frame from Node A (called *initiator*) needs to be transmitted to Node C (called *destination*) with the help of Node B (called *relay*) as shown in Fig. 2. Once the backoff counter of Node A reduces to zero, an RTS frame is sent to Node B as shown in Fig. 10. Besides original contents, this RTS frame also includes the address of the destination (e.g., Node C). After Node B receives this frame, it transmits a CTS frame to the destination (e.g., Node C) and the initiator (e.g., Node A) indicating that they can form ANC cooperation. When the CTS frame is received by Node A, it starts its frame transmission after waiting a short interframe space (SIFS) period. When Node C receives the CTS frame, it also initiates a transmission if there is a data frame to Node A. In this case, the destination (i.e., Node C) is also called a *cooperator*. The frames from the destination

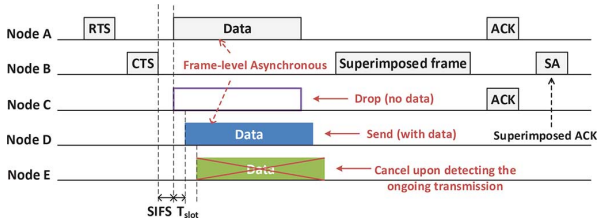

Fig. 10. Flow diagram of the simple random access MAC protocol.

and the initiator superimpose at the relay, and then the relay amplifies and forwards the superimposed signals to the initiator and the cooperator. With RANC, both the initiator and the cooperator can decode their own desired frames, respectively.

2) Flow Compensation: In many cases, Node C may not have a data frame to Node A in its transmission queue when the CTS frame is received. In this scenario, the ANC cooperation cannot be formed since the flow from the destination is absent. Without a cooperator, this situation can significantly reduce the probability of forming ANC cooperation and hence has a negative impact on the network performance. To address this issue, a novel mechanism called *flow compensation* is proposed. Under this mechanism, if Node C does not have a frame to Node A but one of its neighbors, e.g., Node D, coincidentally has one, the traffic from Node D (called *compensator*) can be used to compensate that from Node C to A, i.e., Node D begins to transmit its data frame after receiving the CTS frame. In this case, the data frames from the initiator (e.g., Node A) and the compensator (e.g., Node D) superimpose at the relay node. Following that, the relay node (i.e., Node B) amplifies and forwards the superimposed signals. Based on RANC, Node A can decode the data frame from Node D by canceling the interference from its own frame. Also, if the transmission of Node D is successfully overheard, Node C can utilize RANC to eliminate the interference of the frame from Node D and decode the frame from Node A.

To apply this mechanism, two problems need to be solved. First, given the destination, we need to determine all candidate nodes that can serve as its compensator. Second, given the destination and its compensator candidates, an effective mechanism is required to select an appropriate candidate to form the ANC cooperation with the initiator. The selected candidate compensator must have data frames to the initiator in its transmission queue. Note that each node only has the knowledge about its own queue. It should be noted that, when the CTS frame is being sent, the relay node has no way to identify an appropriate candidate as the compensator. Thus, a sender diversity scheme like that in SourceSync [11] is not applicable.

a) High-Quality Link (HQL) Neighbor Table: To decode the initiator's frames, the destination needs to overhear the transmission of its compensator successfully. For this purpose, each node maintains a special neighbor table called *HQL Neighbor Table*, which contains all neighbors that have a high-quality link[3] to the node. Since the initiator is two hops away from the destination, the signal from a node inside the HQL Neighbor Table of the destination is usually much stronger than that from the initiator. Thus, the destination can successfully overhear the transmission of this node with a high probability. Hence, given the destination, all nodes in its HQL Neighbor Table can serve as its compensator. In addition, each node needs to periodically exchange its HQL Neighbor Table with all of its neighbors.

b) Virtual Contention for Cooperation Opportunity: The second problem in flow compensation can be solved with a virtual contention mechanism as shown in Fig. 10. Specifically, before the transmission of a CTS, the relay node randomly allocates a sequence number within $[0, N-1]$ to the destination and its compensator candidates,[4] where N is the total number of these nodes. Note that the sequence number is different for each node. It indicates the required "backoff time" for each node and is written in a specific field of the CTS frame. Once the CTS is received, the initiator simply starts the transmission of its data frame after waiting for SIFS period, while the destination and its compensator candidates need to contend the transmission opportunity according to their sequence numbers. If a node does not have any data frame to the initiator, it simply drops its transmission opportunity. Otherwise, the node will transmit its data frame upon waiting for $\mathrm{SIFS}+n\cdot T_{\mathrm{slot}}$, where n is the sequence number for the node and T_{slot} is the slot duration. During the waiting time, the node needs to keep overhearing the channel. Once the transmission from another node is detected, the node immediately cancels its own transmission attempt to avoid potential collisions, as shown in Fig. 10. In this way, only one node (e.g., Node D) in the HQL neighbor table is selected as the compensator to form ANC cooperation with the initiator, and the compensator has data frames to the initiator (e.g., Node A). Note that if the sequence number of the compensator is not equal to zero, then the frame from the initiator and that from the compensator will superimpose with several time-slots of asynchronization at the relay node. RANC can effectively support such asynchronization, as it allows fully asynchronous transmissions.

3) Replying ACKs: After decoding the desired frames, the initiator and the destination send ACK frames to report successful receptions. Note that the transmission of ACK frames are also conducted in an ANC cooperation manner, as shown in Fig. 10.

In summary, our protocol exploits signaling messages (e.g., RTS and CTS) to dynamically form ANC cooperation. In this process, no mechanism is required to maintain the synchronization among different nodes since RANC can effectively support asynchronous transmissions. This feature makes our protocol easy to be implemented in real systems. Also, due to the constraint-free characteristics of RANC, the flow compensation mechanism is supported. This mechanism significantly improves the network throughput when traffic flows between different nodes are not symmetric.

4) Resolving the Hidden Terminal Issue: Since three nodes are involved in ANC cooperation, hidden nodes may still exist even if RTS/CTS frames are used. To resolve this issue, we can extend the RTS/CTS mechanism as follows. In Fig. 10, once Node B receives an RTS, instead of sending back a CTS directly

[3]The threshold of link quality is a design parameter depending on the network environment.

[4]Since the HQL Neighbor Table of each node has been broadcast to its neighbors, the relay node has the knowledge of all compensator candidates of the destination.

to Node A, it sends a new short frame called request-to-cooperate (RTC) to Node C. If Node C has data for Node A, then it replies an answer-to-cooperate (ATC) frame to Node B. When Node B receives the ATC frame, it replies a CTS frame to Node A. Since then the ANC cooperation can be started. With the help of RTS, RTC, ATC, and CTS frames, hidden terminals around the three ANC cooperation nodes can be significantly reduced. A complete solution to the hidden terminal issue in a network has been addressed in our recent work [21]. We skip the details here due to page limit.

V. Implementation

A. Platform

All functions of RANC have been implemented in a USRP software radio platform. In this platform, a USRP N210 motherboard with a WBX RF daughter-board operating at 1.26 GHz is used to transmit or receive signals. Via a gigabit Ethernet cable, the USRP device is connected to a general-purpose computer. With the National Instrument (NI) LabVIEW software running on the computer, we implement functions to generate or process baseband signals. The functions specifically designed for RANC are all implemented by ourselves, and standard modules such as modulation/demodulation and channel coding/decoding are adapted from NI's software package.

USRP N210 in our experiment is configured as follows. For the transmitter, the onboard digital-to-analog converter (DAC) chip has a fixed converting rate of 400 M samples per second. We set the interpolation rate to 100 and samples per symbol to 4. The resulting symbol rate is equal to 1 MBd/s. For the receiver, the analog-to-digital convertor (ADC) rate is fixed at 100 M, and samples per symbol is set to 2, which corresponds to $2X$ oversampling in our experiments. To achieve the same symbol rate as that of the transmitter, we set the decimation rate to 50.

B. Communication Nodes

Three types of nodes are implemented for experiments: 1) RANC TX node that generates frames following the format required by RANC; 2) RANC RX node that is capable of decoding superimposed frames; 3) AF node that simply amplifies and forwards received signals.

1) RANC TX Node: A RANC TX node generates frames following the format as mentioned in Section III-A. The default payload size of each frame is 1500 B unless it is specified differently. Two same pilot sequences with the length equal to 160 symbols are attached at the head and the tail of the payload as preamble and postamble. Thus, the total number of pilot symbols is equal to 320, which is identical with that in an 802.11a frame [7]. Moreover, a frame is modulated by BPSK (default), QPSK, 16QAM, or 64QAM and is pulse-shaped with a raised-cosine function. In addition, in the experiments of network applications of RANC, the 1/2 or 3/4 convolutional channel coding is applied.

2) RANC RX Node: A RANC RX node extracts and decodes the desired frame from a superimposed frame. It implements all function blocks shown in Fig. 1.

3) AF Node: An AF node oversamples the received signals and stores the baseband samples without any processing. After receiving a complete superimposed frame, the stored samples are reinterpolated with sinc function, up-converted to the radio frequency, and then transmitted.

Note that in the experiments for network applications of RANC, a single transceiver may play a different role at a different time, i.e., it may serve as a RANC TX node in some time periods but works as a RANC RX node in other time periods.

VI. Performance Evaluation

A. Evaluation on PHY-Layer Performance of RANC

In this section, the physical-layer performance of RANC is evaluated under different scenarios. First, we conduct experiments to demonstrate the necessity and effectiveness of each function block of RANC. Then, the overall BER performance of RANC versus different signal-to-noise ratio (SNR) is measured. The BER corresponds to the decoded frames before channel decoding is performed, and the SNR is defined as $\mathrm{SNR} = |hx|^2/P_{\mathrm{n}}$, where P_{n} is the noise power, h is the channel gain, and x is a symbol signal.

In the PHY-layer experiments, three USRP nodes are involved. Two of them are RANC TX nodes and simultaneously transmit their own frames to a RANC RX node. The RANC RX node has the knowledge about the frame from one of RANC TX nodes and needs to receive the frame from the other one. For each received desired frame, decoding results and related information such as SNR are recoded. If not explicitly specified, we collect the results when the SNR for the desired frame falls into the range of 7–8 dB, which is the typical SNR for BPSK modulation.

1) Frequency Offset: The purpose of the first experiment is to demonstrate that the condition (i.e., $|f_{\mathrm{s}} - f_{\mathrm{s,est}}| \leqslant \frac{\Delta f}{2}$ derived in Section III-E) for our frequency offset algorithm can be practically satisfied.

As discussed in Section III-E, Δf is equal to $\frac{1}{(i_2 - i_1)T}$, where $i_2 - i_1$ is the payload size in symbols and T is the symbol period. In our experiment, since the frame size is 1500 B (i.e., 12 000 symbols for BPSK modulation) and the symbol rate is 1 MBd/s, we have

$$\frac{\Delta f}{2} = \frac{1 \times 10^6}{2 \times 12\,000} = 41.7\,\mathrm{Hz}.$$

Thus, the condition for our frequency offset algorithm becomes $|f_{\mathrm{s,est}} - f_{\mathrm{s}}| < 41.7$ Hz.

To check if the above condition can be satisfied, we measure the actual frequency offset (i.e., f_{s}) between two USRP nodes over 10 s. Each measurement is conducted with an interference-free frame, and the measurements are plotted in Fig. 11. The results show that the frequency offset does not change significantly (much less than 41.7 Hz) within a certain period (e.g., 2 s). Thus, as long as the estimated frequency offset $f_{\mathrm{s,est}}$ in the previous transmission is within the range $\frac{\Delta f}{2}$, its value in the next transmission must be within the same range too. As explained in Section III-E, initially the frequency offset estimation is conducted with an interference-free frame, which means the difference between $f_{\mathrm{s,est}}$ and f_{s} is negligible in the beginning. As a result, the condition for frequency offset estimation is always satisfied through iterative operation of this algorithm.

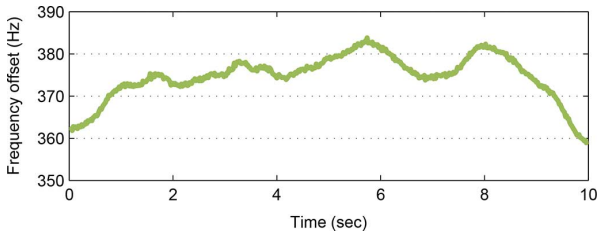

Fig. 11. Variations of frequency offset between two USRP devices over 10 s.

TABLE I
BIT ERROR RATE VERSUS FREQUENCY OFFSET COMPENSATION

Frequency offset	**BER** ($\cdot 10^{-3}$)	
	Long frame (1500 bytes)	Short frame (600 bytes)
No offset	0.664	0.649
Compensated	0.682	0.636
No compensation	35.51	1.751

To evaluate the necessity and effectiveness of our frequency offset estimation scheme, the BER performance of RANC with frequency offset compensation is compared to that of the following two cases: 1) the "no offset" case, where no frequency offset exists between RANC TX nodes and RANC RX nodes; 2) the "no compensation" case, where the frequency offset exists but only preliminary estimation is applied. To eliminate the frequency offset in the "no offset" case, all USRP nodes are connected to a common external oscillator to replace the onboard oscillators. The external oscillator we use is Thunderbolt E GPS disciplined clock [22]. It should be noted that the external oscillator is only used in the "no offset" case for the sole purpose of performance comparison; RANC does not rely on any external oscillator.

The results are shown in Table I, where the "compensated" case represents the normal operation of RANC, i.e., the frequency offset is estimated and compensated without any external oscillator. It can be found that the bit error rate with our frequency offset compensation algorithm is significantly lower than that without compensation, especially when the frame is long and the phase error caused by the residual frequency offset is larger. This difference in BER performance indicates the necessity of our frequency offset compensation algorithm. In addition, according to the table, there does not exist evident difference between the case with our compensation scheme and the case with no frequency offset. This result demonstrates that our frequency offset compensation scheme has effectively eliminated the influence of frequency offset.

2) Joint Channel Estimation: To evaluate the accuracy of joint channel estimation (JCE), we compare the BER performance of our scheme to that of two other cases: 1) no joint channel estimation scenario (i.e., the "Direct" case): the receiver estimates the channel coefficients of the self frame directly, considering the desired frame as interference; 2) interference-free scenario (i.e., the "Free" case): the receiver decodes an interference-free frame. For fair comparison, we collect the results of the three cases where the SNR of the desired frame falls into the same range. Also, in this experiment the self frame and the desired frame have the same length. Thus, the number of effective samples N_{eff} for the self frame is equal to N_{p}, i.e., the

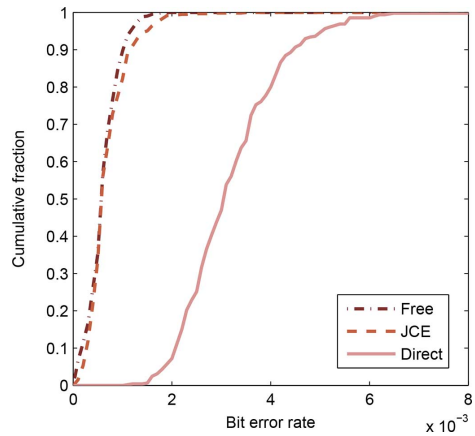

Fig. 12. Bit error rate with joint channel estimation.

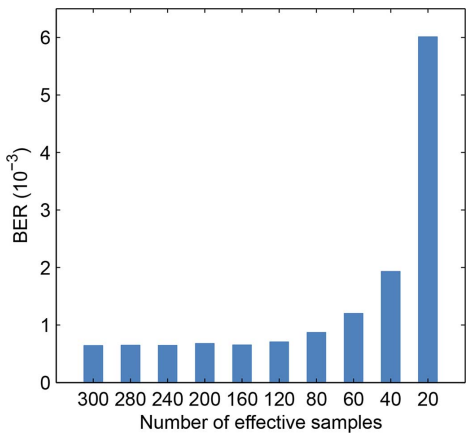

Fig. 13. Bit error rate versus different N_{eff}.

total number of pilot sequences. To conduct this experiment, the frames from two TX nodes are sent asynchronously for many times, and then we look into the scenarios where synchronization of two frames is within 30 symbol times. In these scenarios, the interference-free part of two frames is insufficient for conventional channel estimation (i.e., the "Direct" case).

The cumulative density function (CDF) of BER for the three scenarios are plotted in Fig. 12. It is clear that the BER performance with joint channel estimation closely approaches that of the interference-free scenario. This result indicates that the channel estimation for the self frame is sufficiently accurate so that the residual interference after subtracting the self frame from superimposed signals is negligible. From Fig. 12, we know that the BER of the joint channel estimation scheme is much lower than that with direct channel estimation. Thus, joint channel estimation is necessary when the sufficient interference-free part cannot be guaranteed in a superimposed frame.

To study the impact of N_{eff} on the BER performance, we need to generate superimposed frames with different values of N_{eff}. To this end, we vary the length of the self frames in a specific range and collect the results with N_{eff} very close to (± 3) a specific value labeled on the x-axis of Fig. 13.

The BER performance for different values of N_{eff} is shown in Fig. 13. It can be observed that when N_{eff} reduces to 80,

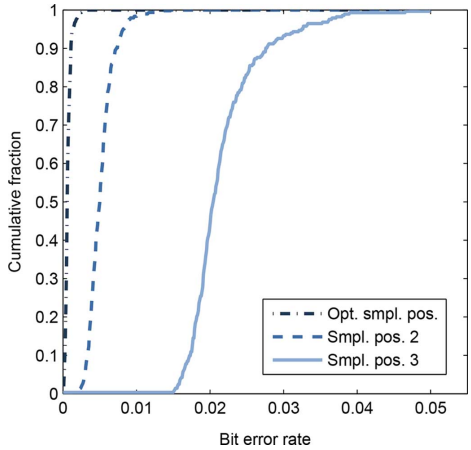

Fig. 14. Bit error rate with or without relocating the optimal sampling positions.

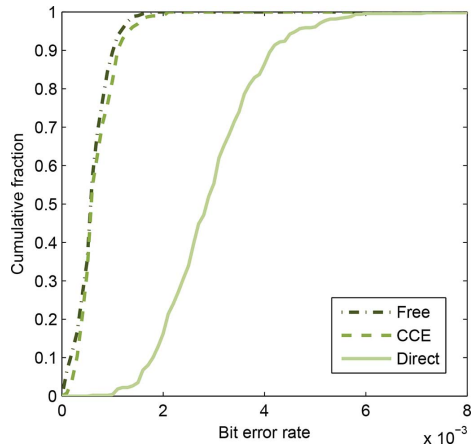

Fig. 15. Bit error rate with circular channel estimation.

the BER performance evidently degrades. As N_{eff} further decreases, the BER performance increases significantly. Based on this figure, the threshold N_{t} (see Section III-A) for selecting joint or circular channel estimation can be determined according to the tolerable degradation of the BER performance. If N_{eff} (which is measured by the frame boundary detection module) is smaller than N_{t}, circular channel estimation is adopted. It should be noted that the threshold N_{t} is not sensitive to the setup of experiments. However, to make it adaptive to different situations, this parameter can be exposed to the MAC driver so that it can be adaptively reconfigured.

3) Waveform Recovery: To examine the necessity of relocating optimal sampling positions in the waveform recovery module, the decoding performance is measured in three different cases. In the first case, resampling is applied, and hence decoding is based on samples at optimal positions. In the other two cases, resampling is disabled, and decoding is conducted directly based on the original samples (at smpl. pos. 2 and smpl. pos. 3) that deviate from the optimal sampling positions. In each case, two TX nodes transmit fixed-length frames with an equal interval time and the RX node keeps receiving the superimposed signals.

The BER performances for the three cases are shown in Fig. 14. It can be found that the BER in the first case is significantly lower than that in the second and third cases. The reason is that the sampling positions in the second and third cases deviate from the optimal positions; without relocating the optimal positions, the equivalent SNRs in these two cases significantly degrade.

4) Circular Channel Estimation: Similar to the experiment for joint channel estimation, circular channel estimation (CCE) is evaluated by comparing the BER performance between RANC with CCE and two other cases: 1) no circular channel estimation scenario (i.e., the "Direct" case); 2) interference-free scenario (i.e., the "Free" case).

The results of the experiment with BPSK modulation are illustrated in Fig. 15. The BER performance significantly degrades if circular channel estimation is not applied. Moreover, the BER performance with circular channel estimation closely approaches that of the interference-free case, which indicates that the circular channel estimation scheme can acquire accurate channel coefficients, and with these coefficients, the self frame can be completely removed from the superimposed signals. Thus, the desired frame is decoded like a nearly interference-free scenario. Note that the CCE scheme in this experiment demands only two rounds of channel estimation.

The performance of circular channel estimation can be influenced by a specific modulation scheme. To investigate this influence, we evaluate the BER performance of circular channel estimation under different modulation schemes. For each modulation scheme, we consider an SNR range in which an interference-free frame can be decoded with a BER of 0.001; no channel decoding is performed. Thus, the SNR of the desired frame falls into the range of [9 dB, 10 dB] for QPSK, [15.5 dB, 16.5 dB] for 16QAM, and [23 dB, 24 dB] for 64QAM.

The results of this experiment are shown in Fig. 16. It can be observed that the maximum performance gain brought by circular channel estimation is more significant for higher order modulation schemes. The reason is that high-order modulations have dense constellation and hence are more vulnerable to the residual self-frame interference caused by inaccurate channel estimation. Thus, the BER performance of high-order modulations degrades more if circular channel estimation is not applied. Also, from Fig. 16, we find that for higher-order modulations, more rounds of channel estimation are required to approach the performance of the interference-free case. This is reasonable because demodulation of the desired frame with a higher-order modulation scheme usually leads to more errors and thus further degrades the accuracy of channel estimation as explained in Section III-D. As a result, more rounds are needed for high-order modulations to get sufficiently accurate channel coefficients for the self frame.

5) BER Performance of RANC: This experiment evaluates the overall BER performance of RANC at different SNR values. To demonstrate that RANC can work without restrictions on superimposed frames, we generate frames on the two TX nodes as follows: 1) frame size varies in the range of [600, 1500] B; 2) the relative delay between two concurrent frames varies from 0 to 1 ms. We set the threshold of effective samples for the self frame (i.e., N_{t}) to 160. Thus, if the number of effective samples

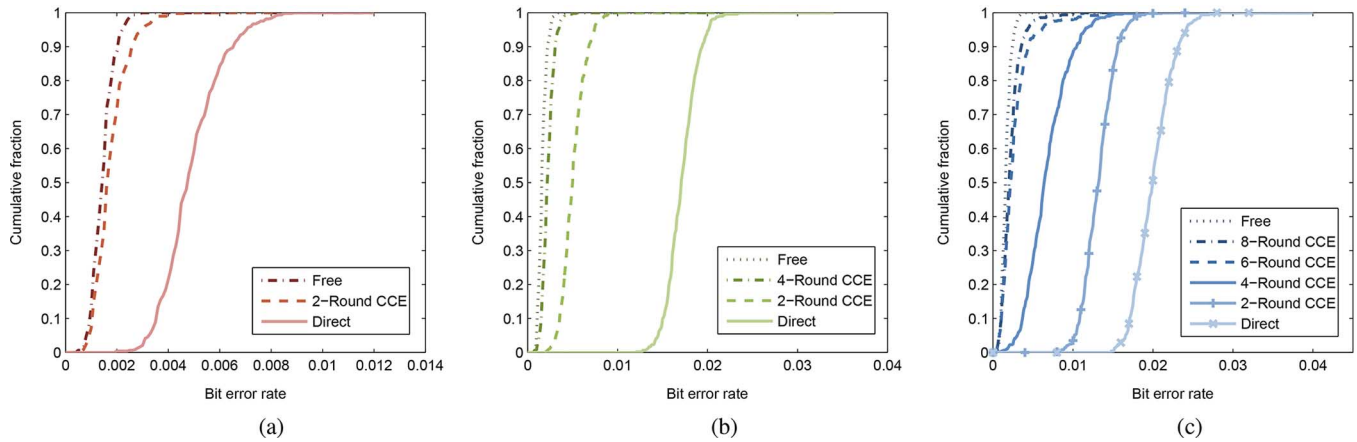

Fig. 16. Circular channel estimation for different modulations. (a) QPSK. (b) 16QAM. (c) 64QAM.

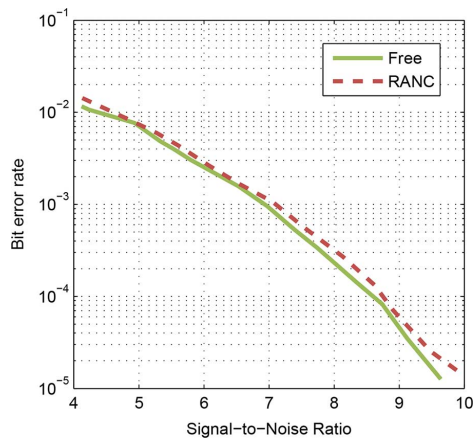

Fig. 17. Bit error rate of RANC under different SNRs.

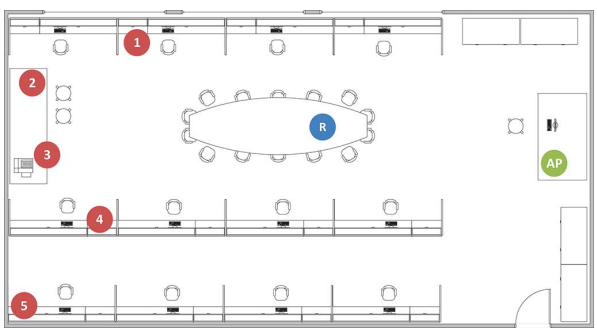

Fig. 18. Node deployment in a laboratory for evaluating multi-way relaying.

is below 160, then circular channel estimation is selected; otherwise, joint channel estimation is adopted.

The results of this experiment are shown in Fig. 17, where the BER performance of the interference-free case is compared. In all SNR regions, the BER performance of RANC closely follows that of the interference-free case, and the performance gap is within 0.3 dB. Thus, the performance advantage of RANC is not restricted to a specific SNR region.

B. Evaluation on Network Applications of RANC

1) Multi-Way Relaying: To demonstrate the advantages of multi-way relaying in wireless networks, the network throughput performance with this scheme is compared to that of two-way relaying in a network as shown in Fig. 18. In this network, there are an access point (AP), a relay node, and five users. The AP needs to transmit data frames to each user, while each user also has traffic flows to the AP. Moreover, we assume that the traffic from the AP to the users and that from the users to the AP are generated by different applications, and hence the sizes of frames in two directions can be different [12]–[14]: The frame from the AP contains the payload of 1500 B, while that from the users has 600 B. All these frames are encoded with 1/2 convolutional channel coding and are modulated with BPSK. Also, the transmission power of each node is adjusted such that its frames can be received by the corresponding destinations with a frame error rate (FER) of less than 10%. With the traditional ANC, such as that in [6], only two-way relaying is supported as discussed in Section IV-A. In this case, we pick each user to exchange data frames with the AP via the relay node in a two-way relaying manner for 400 rounds. We record the decoding results and calculate FERs for each user and the AP. Then, the throughput of each node (the users or AP), which is defined as the number of frames that are successfully transmitted by this node, can be determined. With RANC, multi-way relaying can be effectively supported. In this case, one primary user and one secondary user (20 different combinations in total) are selected in each run. The primary user and the AP exchange their data frames with the help of the relay node, and the secondary user takes the transmission opportunity once the transmission of primary user is finished. For a fair comparison, the frame size, the modulation, and the channel coding for the AP and the users are set identically with those in the two-way relaying case. Also, for each combination of the primary user and the secondary user, 100 rounds[5] of multi-way relaying are conducted. Decoding results of these transmissions are recorded.

a) FER for Overhearing: To decode the frame from the AP, the primary user has to overhear the transmission of the secondary user. The frame error rates for overhearing secondary users by different primary users are shown in Table II. It can be observed that, except for some combinations involving User 5,

[5]The total number of cooperation rounds is equal to 2000, which is the same as that in two-way relaying.

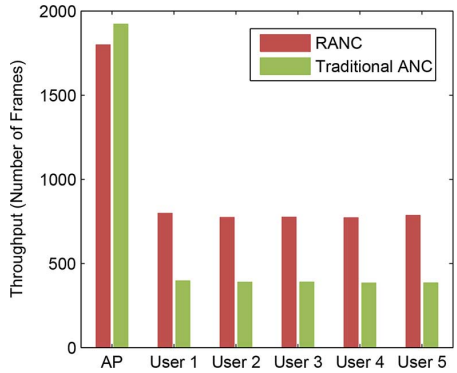

Fig. 19. Throughput comparison between RANC (multi-way relaying) and ANC (two-way relaying).

TABLE II
FRAME ERROR RATE FOR OVERHEARING SECONDARY USERS

Primary user	Frame Error Rate (%)				
	User 1	User 2	User 3	User 4	User 5
User 1	–	0.00	0.00	3.00	9.00
User 2	0.00	–	0.00	0.00	19.0
User 3	0.00	0.00	–	7.00	37.0
User 4	8.00	0.00	0.00	–	0.00
User 5	5.00	16.0	26.0	0.00	–

the FERs for overhearing are always low. This result confirms that when the primary user and the secondary user are close to each other, the signal at the receiver of the primary user is dominated by that from the secondary user, and hence the overhearing is successful with a high probability.

b) Throughput With Multi-Way Relaying: The throughput performance of each node with two-way relaying (supported by traditional ANC) and that with multi-way relaying (supported by RANC) are shown in Fig. 19. The results indicate that the throughput of AP with multi-way relaying is slightly less (about 6%) than that with two-way relaying. This degradation is caused by the occasional failure of overhearing the secondary user. In this case, the frame from AP cannot be successfully received by the primary user. Also, it can be observed that the throughput of each user is almost doubled by adopting multi-way relaying technique. This significant enhancement on throughput attributes to more efficient spectrum utilization of multi-way relaying. For the system overall throughput, the gain from multi-way relaying scheme is about 47%.

2) Random Access With RANC: To evaluate the performance of RANC-based random access MAC protocol (denoted as *R-MAC*) proposed in Section IV-B, the throughput with this protocol is measured in a two-hop network as shown in Fig. 20 where hidden terminals are absent. In this network, the edge nodes (labeled by red dots) at one side (left or right) of the laboratory have traffic flows toward the edge nodes at the other side. Since no direct links exist between the edge nodes at different sides, their data frames need to be forwarded by internal nodes (labeled by green squares). Each data frame is coded with 1/2 or 3/4 convolutional coding and is modulated with BPSK or QPSK according to the link quality.[6] In addition, the payload of a data frame contains 8000 symbols.

[6]The power of each node is set so that there exists no direct link between edge nodes at different sides and link SNRs between edge nodes and internal nodes are around 10 dB. In this case, 16QAM and 64QAM cannot be supported by any link.

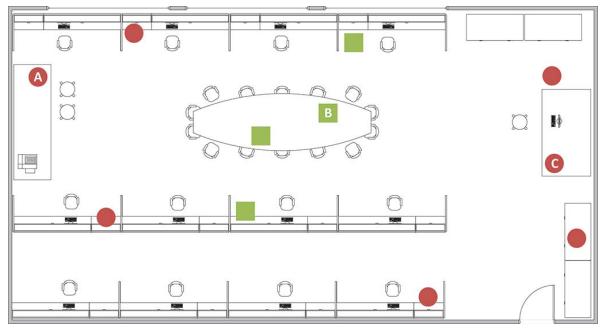

Fig. 20. Node deployment in a laboratory for evaluating R-MAC.

USRP software radio devices cannot support a MAC protocol in real time because most functions of the baseband are still executed in a PC connected to the USRP board. To evaluate the MAC protocol by taking into account the performance of the physical layer, a trace-driven approach is adopted as follows. First, given the network setup shown in Fig. 20, a combination of three nodes (i.e., initiator, relay, and destination) is selected to form ANC cooperation. The RANC-decoding results are measured for the two frames transmitted by the initiator and the destination, respectively. In this combination, we try different coding rates and modulation schemes for both frames, and then the maximum transmission rates for two frames are selected by maintaining the FER to be less than 10%. With the selected rates, the initiator and the destination conduct ANC cooperation for 100 rounds, and the decoding results with RANC are recorded. The same procedure is applied to all combinations of ANC cooperation nodes, and the decoding results are all recorded for use by the MAC-layer emulation. Moreover, for different combinations of three ANC nodes, the reception results are measured and recorded. A similar procedure is applied to the ANC cooperation with flow compensation. In this case, four nodes (i.e., initiator, relay, destination, and compensator) are selected to form ANC, and the reception results are measured and recorded. Note that the measurements for long frames (i.e., data) and short frames (i.e., ACK) are conducted and recorded separately. For comparison, we also measure decoding results for traditional point-to-point transmissions on the links between the initiator, the relay, and the destination with a similar procedure.

Second, with the collected traces of the physical layer, we emulate the MAC behavior in MATLAB. Once an ANC cooperation involving an initiator, a relay, and a destination (may also including a compensator) is formed following our MAC protocol, the corresponding decoding results are retrieved randomly from one of the 100 records corresponding to this set of three-node ANC. Based on these results, the MAC protocol proceeds to the next step. Similarly, the standard IEEE 802.11 MAC is also emulated with the measured traces of point-to-point transmissions. The protocol parameters used in the emulation are summarized in Table III. They are selected by referring to IEEE 802.11a standard [7]. However, since the symbol rate of the physical-layer experiments is 1/20 of that specified in [7], the time-related parameters are scaled down by 20 times as shown in [7]. Also, the RTS frame and CTS frame in our protocol contains more information, and therefore the sizes of these

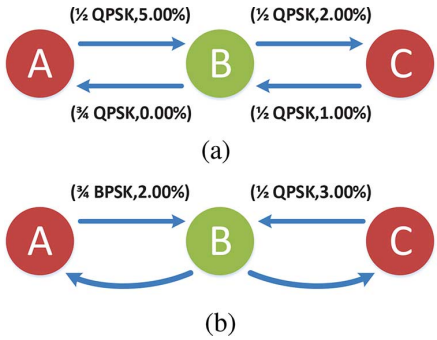

Fig. 21. The transmission rates and the FER for different physical-layer techniques. With these rates and FER, the average throughput for point-to-point transmissions is 0.539 M/s, while that for RANC is 0.853 M/s. (a) Point-to-point transmission, (b) RANC.

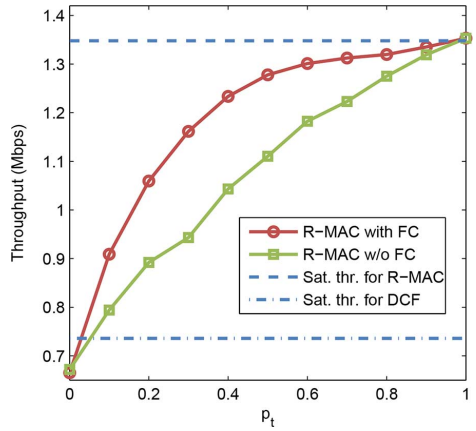

Fig. 22. Throughput performance with R-MAC.

TABLE III
PROTOCOL PARAMETERS USED IN THE EXPERIMENTS

Protocol Parameters			
Item	Value	Item	Value
symbol rate	1 MBd/s	payload	8 ms
PHY header (PH)	400 μs	SIFS	320 μs
RTS	320 μs + PH	DIFS	680 μs
CTS	224 μs + PH	slot time	180 μs
ACK	224 μs + PH	init. window size	64 slots
RTS (R-MAC)	416 μs + PH	max. backoff stage	3
CTS (R-MAC)	512 μs + PH		

frames are longer than those in IEEE 802.11a. The backoff stage is smaller than the standard number because of a small number nodes in the network.

a) Noise Accumulation: Since ANC cooperation involves amplify-and-forward process, the influence of noise accumulation on the decoding performance needs to be considered. To illustrate this influence in our experiment, the decoding results for a combination of an initiator, a relay, and a destination is shown in Fig. 21, where the maximum supported transmission rate (expressed as the combination of modulations and coding schemes) and the frame error rate are labeled on each link. It can be observed that transmitters have to reduce their rates to utilize ANC cooperation due to the existence of noise accumulation. Taking this rate degradation into account, the throughput performance gain with ANC cooperation in a two-way relay channel is about 60% instead of 100% in an ideal scenario (i.e., no noise accumulation).

b) Saturation Throughput: To evaluate the maximum throughput that can be supported in a network with ANC cooperation, the saturation throughput with our MAC protocol is measured. Here, the network throughput is defined as the successfully transmitted payload bits on all links in a second, and the saturation scenario indicates that any edge node at one side (left or right) of the laboratory always has data frames to any edge node at the other side. The saturation throughput (sat. thr.) of our MAC protocol is shown in Fig. 22. For comparison, the saturation throughput of the IEEE 802.11 DCF is also provided. It can be observed that the performance gain with our MAC protocol is close to 80%. This significant improvement in throughput is attributed to two factors. First, ANC cooperation improves the spectrum utilization compared to the traditional point-to-point transmissions. According to the previous results, this brings about 60% throughput enhancement. Second, for each transmission round (i.e., from the start of an RTS to the end of replying ACKs), the effective data transmission time in our MAC protocol, including data transmission time of edge nodes and the amplify-and-forwarding time of internal nodes, is much longer than that of the IEEE 802.11 DCF. Therefore, the overhead in each transmission round (caused by contention, backoff, and control frames such as RTS/CTS) accounts for a lower percentage in our MAC protocol.

c) Flow Compensation: In more realistic scenarios, an edge node at one side of the laboratory does not always have data frames to each edge nodes at the other side. In this case, the flow compensation mechanism is necessary to improve the network performance as discussed in Section IV-B. To evaluate the effectiveness of this mechanism, the network throughput is compared to that without the mechanism. To consider different degrees of asymmetrical flows, the probability (denoted as p_t) that an edge node has a data frame to the initiator varies from zero to one. The throughput results are shown in Fig. 22. When p_t is close to zero, the ANC cooperation is hardly formed even with the flow compensation mechanism, so the throughput is slightly improved. When p_t is close to 1, the ANC cooperation can be easily formed even if the flow compensation mechanism is not applied. Except for these two extreme cases, the flow compensation mechanism can significantly improve the throughput performance.

In our network setting, the HQL Neighbor Table of an edge node only contains one or two members. If a node has more neighbors and hence a larger HQL Neighbor Table, more candidates can compensate the traffic flows from the destination, and the probability of forming ANC cooperation will further increase. In this case, the performance gain brought by the flow compensation mechanism is even larger.

VII. RELATED WORK

ANC [1] and PLNC [23] can achieve higher spectrum efficiency than a traditional network coding scheme, as explained

in [24]. A constraint for applying these techniques is the requirement of both frame-level and symbol-level synchronization, which is highly difficult to achieve in many application scenarios. To address this issue, an ANC scheme [6] and several OFDM-based PLNC schemes [2]–[4] are developed. However, these schemes are still limited by other constraints as discussed in Section II. In contrast, RANC has eliminated all these constraints.

Several other papers have also studied ANC or PLNC by considering asynchronously superimposed frames. In [25], an asynchronous PLNC based on belief propagation is proposed. However, this scheme requires the precise knowledge of the time offset between arrivals of two concurrent frames. This is difficult to acquire in many communication systems. A convolutional channel coding scheme is developed in [26] to support asynchronous PLNC. In this scheme, the two concurrent frames adopt a channel coding scheme with the same coding rate. This is generally impractical, as the rate adaption algorithm in a communication system can easily lead to a different coding rate on a different communication node. Another ANC scheme for an asynchronous two-way relay network is proposed in [27], but it is focused on how to achieve full diversity among multiple relay nodes; interference from the self frame is assumed to be perfectly canceled. In [28], an OFDM-based PLNC is implemented. Asynchronization of two transmitting frames needs to be smaller than the CP, which has a length of 16 samples. The measurement results from implementation prove that, as long as the asynchronization of two transmitting frames is less than the CP of an OFDM symbol, PLNC can be properly done. In a system with a wide bandwidth, the CP can be very short. For example, in a 20-MHz system, the CP can be smaller than 1 μs. Achieving such a synchronization accuracy is difficult in an asynchronous wireless network. Therefore, the solution in [28] cannot guarantee its applicability to real systems. The constraints or ideal assumptions for applying ANC in the aforementioned schemes do not exist in RANC.

Besides analog network coding schemes, there are other mechanisms developed to extract the desired frames from superimposed signals. One category of such mechanisms is message-in-message (MIM) reception. The schemes [29]–[31] in this category get the desired frames by considering the physical-layer capture effect [32], [33]. To this end, the signal strength of one frame in the superimposed signals needs to be significantly stronger than that of the other one. In contrast, RANC works in the cases where two concurrent frames have comparable signal strength. Actually, RANC and MIM schemes are complementary: When the signal strength of the two frames in the superimposed signals are comparable, RANC is applied to extract the desired frame. However, if the physical-layer capture effect can be leveraged, an MIM scheme can be adopted.

Moreover, a ZigZag decoding scheme proposed in [16] also utilizes superimposed signals to obtain the desired frames. This scheme considers two superimposed waveforms, and the frame offsets in the two superimposed waveforms need to be different. However, RANC and other ANC schemes consider only one superimposed waveform from two frames (one of which is assumed to be known). Hence, the application scenarios of ZigZag and RANC are different.

VIII. Conclusion

In this paper, a restriction-free analog network coding (RANC) scheme was developed to achieve fully asynchronous transmissions. It supports all linear modulation schemes. Moreover, unequal frame sizes in the concurrent transmissions work perfectly in RANC. The advantages of RANC make it highly flexible and efficient for being applied to a wireless network. To demonstrate this feature, two network applications of RANC were studied. Such applications are not feasible without the support of RANC. RANC and its applications were implemented on a software radio testbed, and extensive experiments proved that RANC worked gracefully without being constrained by synchronization, frequency offset, modulations, and frame size. With RANC, the BER performance of receiving the desired frame from the superimposed signals is comparable to that of interference-free communications. Experiments in a real network setup demonstrated that RANC outperformed the existing ANC schemes and significantly enhanced the network throughput. Due to the restriction-free nature, RANC is promising to support more creative applications of analog network coding in wireless networks.

Acknowledgment

The authors would like to thank the financial sponsors for their generous support.

References

[1] P. Popovski and H. Yomo, "Bi-directional amplification of throughput in a wireless multi-hop network," in *Proc. IEEE VTC*, 2006, pp. 588–593.

[2] F. Rossetto and M. Zorzi, "On the design of practical asynchronous physical layer network coding," in *Proc. IEEE SPAWC*, 2009, pp. 469–473.

[3] Z. Li and X.-G. Xia, "A simple Alamouti space-time transmission scheme for asynchronous cooperative systems," *IEEE Signal Process. Lett.*, vol. 14, no. 11, pp. 804–807, Nov. 2007.

[4] Z. Li and X.-G. Xia, "An Alamouti coded OFDM transmission for cooperative systems robust to both timing errors and frequency offsets," *IEEE Trans. Wireless Commun.*, vol. 7, no. 5, pp. 1839–1844, May 2008.

[5] J. Elson, L. Girod, and D. Estrin, "Fine-grained network time synchronization using reference broadcasts," *Oper. Syst. Rev.*, vol. 36, no. SI, pp. 147–163, 2002.

[6] S. Katti, S. Gollakota, and D. Katabi, "Embracing wireless interference: Analog network coding," in *Proc. ACM SIGCOMM*, 2007, pp. 397–408.

[7] *IEEE Standard for Information Technology Part 11: Wireless LAN Medium Access Control (MAC) and Physical Layer (PHY) Specifications: High-Speed Physical Layer in the 5 GHz Band*, IEEE Std 802.11a, 1999, p. 24.

[8] B. Sundararaman, U. Buy, and A. D. Kshemkalyani, "Clock synchronization for wireless sensor networks: A survey," *Ad Hoc Netw.*, vol. 3, no. 3, pp. 281–323, 2005.

[9] P. Sommer and R. Wattenhofer, "Gradient clock synchronization in wireless sensor networks," in *Proc. IEEE IPSN*, 2009, pp. 37–48.

[10] *IEEE Standard for Information Technology Part 11: Wireless LAN Medium Access Control (MAC) and Physical Layer (PHY) Specifications Amendment 3: Enhancements for Very High Throughput in the 60 GHz Band*, IEEE Std 802.11ad, 2012, pp. 1–628.

[11] R. Hariharan, H. Hassanieh, and D. Katabi, "SourceSync: A distributed wireless architecture for exploiting sender diversity," in *Proc. ACM SIGCOMM*, 2010, pp. 171–182.

[12] A. McGregor, M. Hall, P. Lorier, and J. Brunskill, "Flow clustering using machine learning techniques," in *Proc. Passive Active Netw. Meas.*, 2004, pp. 205–214.

[13] M. Roughan, S. Sen, O. Spatscheck, and N. Duffield, "Class-of-service mapping for QoS: A statistical signature-based approach to IP traffic classification," in *Proc. ACM IMC*, 2004, pp. 135–148.

[14] Y.-D. Lin, C.-N. Lu, Y.-C. Lai, W.-H. Peng, and P.-C. Lin, "Application classification using packet size distribution and port association," *J. Netw. Comput. Appl.*, vol. 32, no. 5, pp. 1023–1030, 2009.
[15] K. Jamieson and H. Balakrishnan, "PPR: Partial packet recovery for wireless networks," in *Proc. ACM SIGCOMM*, 2007, pp. 409–420.
[16] S. Gollakota and D. Katabi, "Zigzag decoding: Combating hidden terminals in wireless networks," in *Proc. ACM SIGCOMM*, 2008, pp. 159–170.
[17] K. Tan *et al.*, "SAM: Enabling practical spatial multiple access in wireless LAN," in *Proc. ACM MobiCom*, 2009, pp. 49–60.
[18] U. Mengali and A. N. D'Andrea, *Synchronization Techniques for Digital Receivers*. New York, NY, USA: Springer, 1997.
[19] W. Mao and X. Wang, "Random analog network coding," 2014 [Online]. Available: http://wanglab.sjtu.edu.cn/userfiles/files/ranc_original.pdf
[20] P. H. W. Fung, S. Sun, and C. K. Ho, "Preamble design for carrier frequency offset estimation in two-way relays," in *Proc. IEEE SPAWC*, 2010, pp. 1–5.
[21] W. Mao and X. Wang, "ANC-ERA: Random access for analog network coding in wireless networks," 2014 [Online]. Available: http://wanglab.sjtu.edu.cn/userfiles/files/ANCERA.pdf
[22] Trimble, Inc., Sunnyvale, CA, USA, "Thunderbolt E GPS disciplined clock," [Online]. Available: http://www.trimble.com/timing/thunderbolt-e.aspx
[23] S. Zhang, S. C. Liew, and P. P. Lam, "Hot topic: Physical-layer network coding," in *Proc. ACM MobiCom*, 2006, pp. 358–365.
[24] B. Rankov and A. Wittneben, "Spectral efficient protocols for half-duplex fading relay channels," *IEEE J. Sel. Areas Commun.*, vol. 25, no. 2, pp. 379–389, Feb. 2007.
[25] L. Lu, S. C. Liew, and S. Zhang, "Optimal decoding algorithm for asynchronous physical-layer network coding," in *Proc. IEEE ICC*, 2011, pp. 1–6.
[26] D. Wang, S. Fu, and K. Lu, "Channel coding design to support asynchronous physical layer network coding," in *Proc. IEEE GLOBECOM*, 2009, pp. 1–6.
[27] H.-M. Wang, X.-G. Xia, and Q. Yin, "A linear analog network coding for asynchronous two-way relay networks," *IEEE Trans. Wireless Commun.*, vol. 9, no. 12, pp. 3630–3637, Dec. 2010.
[28] L. Lu, T. Wang, S. C. Liew, and S. Zhang, "Implementation of physical-layer network coding," *Phys. Commun.*, vol. 6, p. 74 C87, Mar. 2013.
[29] J. Lee *et al.*, "An experimental study on the capture effect in 802.11a networks," in *Proc. ACM WinTECH*, 2007, pp. 19–26.
[30] T. Nadeem and L. Ji, "Location-aware IEEE 802.11 for spatial reuse enhancement," *IEEE Trans. Mobile Comput.*, vol. 6, no. 10, pp. 1171–1184, Oct. 2007.
[31] J. Manweiler *et al.*, "Order matters: Transmission reordering in wireless networks," *IEEE/ACM Trans. Netw.*, vol. 20, no. 2, pp. 353–366, Apr. 2012.
[32] A. Kochut, A. Vasan, A. U. Shankar, and A. Agrawala, "Sniffing out the correct physical layer capture model in 802.11b," in *Proc. IEEE ICNP*, 2004, pp. 252–261.
[33] M. Durvy, O. Dousse, and P. Thiran, "Modeling the 802.11 protocol under different capture and sensing capabilities," in *Proc. IEEE INFOCOM*, 2007, pp. 2356–2360.

Xudong Wang (S'00–M'03–SM'08) received the Ph.D. degree in electrical and computer engineering from the Georgia Institute of Technology, Atlanta, GA, USA, in 2003.

He is currently with the University of Michigan–Shanghai Jiao Tong University (UM-SJTU) Joint Institute, Shanghai Jiao Tong University, Shanghai, China. He is a Distinguished Professor (Shanghai Oriental Scholar) and is the Director of the Wireless and NetworkinG (WANG) Lab. He is also an affiliate faculty member with the Electrical Engineering Department, University of Washington, Seattle, WA, USA. Since receiving the Ph.D. degree, he has worked as a Senior Research Engineer, Senior Network Architect, and R&D Manager with several companies. He has been actively involved in R&D, technology transfer, and commercialization of various wireless networking technologies. He holds several patents on wireless networking technologies and most of his inventions have been successfully transferred to products. His research interests include wireless communication networks, smart grid, and cyber-physical systems.

Dr. Wang is an Editor for the IEEE TRANSACTIONS ON MOBILE COMPUTING, IEEE TRANSACTIONS ON VEHICULAR TECHNOLOGY, and *Ad Hoc Networks*. He was the Demo Co-Chair of the ACM International Symposium on Mobile Ad Hoc Networking and Computing (ACM MobiHoc 2006), a Technical Program Co-Chair of the Wireless Internet Conference (WICON) 2007, and a General Co-Chair of WICON 2008. He has been a technical committee member of many international conferences.

Wenguang Mao received the B.S. degree in electrical and computer engineering and M.S. degree in information and communication engineering from Shanghai Jiao Tong University (SJTU), Shanghai, China, in 2011 and 2014, respectively.

His current research interests include MAC protocols, physical-layer cooperative coding schemes, and mobile applications in smartphones and wearable computers.